FLAVOR FLOW SIGNATURES OF QUARK-GLUON PLASMA

JOHANN RAFELSKI

Department of Physics, University of Arizona, Tucson, AZ 85721

JEAN LETESSIER and AHMED TOUNSI

Laboratoire de Physique Théorique et Hautes Energies
Université Paris 7, Tour 24, 2 Pl. Jussieu, F-75251 Cedex 05, France

Theoretical considerations show that in the deconfined quark-gluon plasma (QGP) phase high local strange and antistrange particle density is reached. This observation has inspired investigation of strange particle production as a signature of QGP formation in relativistic heavy ion collisions. Currently, the primary experimental interest is centered on otherwise rarely produced strange antibaryons. We present here a self-contained introduction to the subject matter: we describe and justify the model assumptions, present the highlights of the experimental results motivating the theoretical developments, introduce in considerable detail the theoretical calculations of strangeness production and present a comprehensive data interpretation, within the thermal fireball model. Among novel results presented we draw attention to the exploration of the time and temperature evolution of the strangeness and charm phase space occupancy.

1 Relativistic Heavy Ion Collisions

Our objective is to study conditions akin to those prevailing during the era of the Early Universe at which temperatures were in excess of 200 MeV, less than $10\,\mu$s after the big bang. Our specific objective is to explore a new form of matter, the quark-gluon plasma (QGP). Heaviest nuclei at relativistic energies are the tools in this research program: in their collisions the participating strongly interacting (hadronic) nuclear matter is compressed and heated. Our hope and expectation is that in the collisions of large nuclei which we consider here, pieces of nuclear matter large enough to allow us to explore infinite systems of hot hadronic matter are formed, thus permitting us to employ the great simplicity arising for statistical systems. It is widely believed that at these extreme conditions the nature of the vacuum state of strong interactions is changed allowing for the free propagation of quark and gluon color charges.[1] The discovery of the QCD-vacuum 'melting' and the study of the properties of the perturbative and true vacuum is, in our view, the primary fundamental theoretical objective of the nucleus-nucleus high energy collision experimental program — high energy nuclear collisions are today the only known method allowing the study of extended space-time regions containing a locally modified vacuum state.

Relativistic heavy ion experimental programs at the AGS accelerator at Brookhaven National Laboratory (BNL) and at the SPS accelerator at European Center of Nuclear Research (CERN) in Geneva, begun in 1986–87, following on several years of preparation. From the onset of the heavy ion collision research program it was

believed that the higher the collision energy and the heavier the colliding nuclei, the greater the energy density that could be created and hence more extreme conditions of matter and, e.g., earlier the time since the beginning of our Universe one expects to be able to study. The next generation of experiments will exploit the RHIC facility, the 100A+100A GeV heavy ion collider at BNL. RHIC will deliver at the end of the century 10 times the CM-energy available today at SPS. At CERN, the recently approved LHC facility is designed to permit collisions of heavy ions up to about 2.5A+2.5A TeV. Here yet considerably more extreme conditions will be reached as the collision energies are 20–30 times higher than accessible at RHIC, 200–300 times greater than what we study today at SPS and 1000 times above the current BNL experiments. The expected onset of the LHC program follows RHIC schedule by about 5 years.

This paper is devoted to the study of hadronic signatures involving specifically the production and evolution of the strange quark flavor[2] in this new hadronic color deconfined phase. Inside the domain of perturbative vacuum, at sufficiently high excitation energy, we expect to encounter a quantum gas of quarks and gluons subject to the QCD perturbative interactions characterized by the (running) coupling constant α_s. The moderate magnitude $\alpha_s/\pi \leq 0.2$ at the energy scales corresponding to temperatures of $T \simeq 250$ MeV should permit us to study the quark matter in a first estimate of its properties, as if it consisted of a gas of quarks and gluons interacting perturbatively. For example, we consider perturbative QCD strangeness production, and also use perturbative QCD to improve the free quantum gas equations of state. We use the analytical expressions up to the region of the phase cross-over to the confined hadronic gas world, hoping that the qualitative features of the deconfined phase will be appropriately described in that way. Clearly, this is the domain that will see in future more effort both in terms of improvements of the perturbative expressions, and also due to further exploration of numerical lattice gauge theory results.[1]

In the deconfined QGP phase we find enhanced production of strangeness flavor by glue based processes. This leads to enhanced strange particle abundances in the final state, and more specifically, to an enhanced production of strange antibaryons.[3] This signature of QGP requires that the transition from the deconfined state to the confined final hadronic gas phase consisting of individual hadrons occurs sufficiently rapidly in order that the memory of the high density of strangeness in the early phase which generates this highly anomalous yields of multiply strange particles is not erased. The (enhanced) production of (multi)strange antibaryons is considered to be more specifically related to deconfinement than are other strange particle observables, because of the large difference in chemical equilibration time scales and chemical properties in the deconfined quark-gluon and hadronic-gas (HG) phases.

The final state observable 'strangeness' is more than just one quantity which is enhanced by a factor two or two and a half when one compares usual nucleon–nucleon (N–N) and nucleon–nuclei (N–A) with nuclei–nuclei (A–A) reactions. The interesting aspects of this observable are that certain strange particles appear much more enhanced than others, since their production is rather suppressed in conventional interactions. Moreover, the particle production mechanisms being very different from

2

the usual ones, the behavior of the yields (cross sections) with energy can be expected to deviate from expectations.

We think that our recent advances[4,5] in the study of strange particle production have brought about the long aspired substantiation of the formation of deconfined and nearly statistically equilibrated QGP phase in sufficiently high energy nuclear collisions, here in particular at energies available at the SPS accelerator, $\sqrt{s_{NN}} \simeq 9 + 9$ GeV. We reach this conclusion because the observed abundances of strange antibaryons are closely following the expected pattern[6] characteristic for a rapidly hadronising deconfined phase, at the same time as an excess of entropy[7] characteristic for melted hidden (color) degrees of freedom is recorded.

We begin in section 2 with a brief introduction to thermal fireball model, which provides us with the general framework for the theoretical modeling of the dynamics of nuclear collisions and the QGP formation, properties and evolution. We then survey in section 3 the key experimental results obtained at SPS. In section 4 we study the conditions which we expect to be formed in different collisions. We then turn our attention in section 5 to a comprehensive study of the QCD–QGP based thermal strangeness production and also discuss briefly the related topics of the thermal charm production. In section 6 we explore the variation of the phase space occupancy of strange and charmed particles in the different collision environments. We discuss the hadronisation constraints and parameters in section 7, and present the excitation functions of multi-strange particle ratios obtained within our model in section 8. In the final section 9 we give a brief summary of our work.

We wish to stress that the observation of a transient new phase of matter is only possible if the quantum coherence and thus time reversibility of the collision process is broken, which is presumed in our work, e.g. when we introduce entropy production by assuming thermalization of the initial state. Why and how this occurs is one of the greatest mysteries of the subject matter.

2   Thermal Models

Many experimental results, of which some will be discussed here, strongly suggest that the particles produced in heavy ion collisions are indeed thermal, that is either they have been produced by a thermal source, for example in a recombination of thermal constituents, or that they have had time to scatter and thermalize after formation. This also means that we assume that the thermalization of the energy content in heavy ion reactions is rapid on the time scale of the collision. The required mechanisms of such a rapid thermalization and associated entropy production are today still unknown. But once this hypothesis is made, the remaining issue and thus our primary attention addresses the description of the time evolution of chemical properties, e.g., particle content.

The special virtue of the thermal fireball framework we develop is that the spectra and particle abundances can be described in terms of a few parameters which have very intuitive meaning. In this the thermal model analysis of the experimental re-

sults differs fundamentally from other efforts made with individual particle cascade type models. These contain as inputs detailed data and their extrapolations, and often also assumptions about unknown reaction cross sections. The attainment of thermal equilibrium is in these calculations result of many individual particle-particle collisions. However, for the N–N collisions we already know that the appearance of the thermal particle distributions in the final state is inexplicable in terms of dynamical microscopic models.[8] Consequently, there is no reason to expect that some microscopic dynamical approach, invoking multiple series of N–N type interactions, leads to any better understanding of the thermalization process. Moreover, if the underlying and yet not understood thermalization processes are, as is likely in view of the N–N situation, much faster than those operating in the numerical cascade codes, these results would not be adequate.

Such an uncertainty about the microscopic mechanisms does not beset the thermal approach, where we do not implement a microscopic mechanism for thermalization, but rather analyze the data assuming that, though not understood, thermalization is the fastest, nearly instantaneous, hadronic process. The prize one pays in this approach is that, under certain conditions, one looses the ability to describe some details of the collision evolution. For example, we have not been able to identify within a thermal model a method to determine the stopping fractions (i.e. energy or baryon number deposition rate) governing the different collisions and we extract this parameter in qualitative form from the data. In the microscopic models one can in principle claim to 'derive', e.g., the energy-momentum stopping. This current deficiency of the thermal model disappears under conditions which could lead to full stopping. In the near future we will see up to which energy this may occur for the Pb–Pb reactions. The initially studied maximum energy is 158A GeV and we hope that in a very near future the energy range between 40A and 158A GeV can be explored.

It should be noted here that in a rough survey of the particle yields one aught to observe the considerable impact of the surface of the colliding nuclei, always present in symmetric systems. Consequently, it is no surprise that many observed particle rapidity yields are wider than expected even in presence of full stopping — the degree of stopping reached can be more effectively explored considering the rapidity shapes of particles which cannot be easily made in single hadron interactions (e.g. $\overline{\Lambda}$).

We now discuss in qualitative terms the global parameters of the thermal fireball model. When studying particle spectra it is convenient to introduce instead of the longitudinal momentum, the rapidity y and to use the transverse mass $m_\perp$ instead of the transverse momentum of a particle:

$$y = \frac{1}{2} \ln \left(\frac{E + p_z}{E - p_z} \right), \qquad E = m_\perp \cosh y, \qquad m_\perp = \sqrt{m^2 + p_\perp^2}, \qquad (1)$$

where '$\perp$' is perpendicular to the collision axis 'z'. While $m_\perp$ is invariant under Lorentz transformations along the collision axis, the particle rapidity y is additive, that is it changes by the constant value of the transformation for all particles. This allows to choose the suitable (CM — center of momentum) reference frame characterized by its rapidity y_{CM} for the study of the particle spectra.

We suppose that the primordial source is a space-time localized region of thermal hadronic matter which is the source of all particle Boltzmann type spectra. At relatively high $m_\perp$ the exponential spectral shape is relatively little deformed by resonance decay and the fireball dynamics, here in particular flow phenomena. Thus this portion of the spectrum should be similar for different particles, which would allow a reduction of all data to just one basic spectral shape form:

$$\frac{d^3N}{dp^3} = N_i e^{-E^{(i)}/T} = N_i e^{-\cosh(y-y_{\mathrm{CM}})\, m_\perp^i/T} \,. \tag{2}$$

The parameters of each particle distribution include the inverse slope T ('temperature') of the $m_\perp$ distribution, centered around the y_{CM}.

The fireball is created in central symmetric collisions at the CM-rapidity of the N–N system, which is for relativistic systems just is $1/2$ of the projectile rapidity. For asymmetric collisions such as S–Au/W/Pb the CM rapidity depends on the ratio of the participating masses A_{P}, A_{T} of the projectile and, respectively, target nuclei. Simple kinematic considerations show that the center of momentum frame is at[11,12] (neglecting small corrections):

$$y_{\mathrm{CM}} = \frac{y_{\mathrm{P}}}{2} - \frac{1}{2}\ln\frac{A_{\mathrm{T}}}{A_{\mathrm{P}}}\,. \tag{3}$$

Assuming small impact parameter collisions with a suitable central trigger, all projectile nucleons participate while the target participants A_{T} can be estimated from a geometric 'interacting tube' model. This approach reproduces well the value of rapidity around which the particle spectra are centered (central rapidity) in the specific case of 200A GeV S–Au/W/Pb interactions. We find $y_{\mathrm{CM}} = 2.6 \pm 0.1$, the uncertainty arising from the impact parameter averaging and variations of the surface nucleon participation. On the other hand, once the central rapidity is experimentally confirmed, the ratio of participating projectile and target masses is known allowing the determination of the CM-energy involved in the interaction.

The relative abundance of particles emerging from the thermal fireball is controlled by the chemical (particle abundance) parameters, the particle fugacities,[4] which allow to conserve flavor quantum numbers. Four fugacities are introduced since the flavors u, d, s and as appropriate c are separately conserved on the time scale of hadronic collisions and can only be produced or annihilated in particle-antiparticle pair production processes[a]. The fugacity of each hadronic particle species is the product of the valence quark fugacities, thus, for example, the hyperons have the fugacity $\lambda_{\mathrm{Y}} = \lambda_{\mathrm{u}}\lambda_{\mathrm{d}}\lambda_{\mathrm{s}}$. Fugacities are related to the chemical potentials μ_i by:

$$\lambda_i = e^{\mu_i/T}\,, \quad \lambda_{\bar{\imath}} = \lambda_i^{-1} \qquad i = u,\, d,\, s\,. \tag{4}$$

---

[a]We will in general not introduce and/or discuss the fugacities for quarks heavier than s. While we explore in qualitative terms the charm production, it remains a rather small effect even at LHC energies.

Therefore, the chemical potentials for particles and antiparticles are opposite to each other, provided that there is complete chemical equilibrium, and if not, that the deviation from the full phase space occupancy is accounted for by introducing a non-equilibrium chemical parameter γ (see below).

In many applications it is sufficient to combine the light quarks into one fugacity

$$\lambda_q^2 \equiv \lambda_d \lambda_u \,, \quad \mu_q = (\mu_u + \mu_d)/2 \,. \tag{5}$$

The slight isospin asymmetry in the number of u and d quarks is described by the small quantity

$$\delta\mu = \mu_d - \mu_u \,, \tag{6}$$

which may be estimated by theoretical considerations.[4]

Since a wealth of experimental data can be described with just a few model parameters, this leaves within the thermal model a considerable predictive power and a strong check of the internal consistency of the thermal approach we develop. Specifically, in the directly hadronising off-equilibrium QGP-fireball considered here there are 5 particle multiplicity parameters (aside of T and y_{CM}) characterizing all particle spectra: the fireball size V, two fugacities λ_q, λ_s, of which the latter one is not really a parameter in our approach, as we will set $\lambda_s = 1$ because of strangeness conservation in the QGP phase, and two particle abundance non-equilibrium parameters we will discuss at length below: the strangeness occupancy factor we call γ_s and the ratio R_C^s, see Eq. (79), of meson to baryon abundances normalized to hadronic gas equilibrium. Only the last of these parameters is related to the mechanism governing the final state hadronisation process, the others will be determined using a dynamical picture of the collision, in which the input is derived from more general qualitative conditions of the colliding system, such as the energy content or stopping power. Thus the validity of thermal and (approach to) chemical equilibrium can be conclusively tested, comparing the observed particle spectra and yields with the theoretical predictions, without the need or even capability to modify and adapt the theoretical description to each new experimental result, as we see this done in the microscopic dynamical (cascade type) models.

We now look at the different stages of the temporal evolution[13] and the related parameters of the fireball. The scenario we adopt is in view of the current understanding of hadronic physics the most natural one in qualitative terms, in accord with the general properties of the strong interactions and hadronic structure widely known and accepted today, and as we shall see, it is also in quantitative agreement with experimental results obtained in relativistic nuclear collisions.

When studying collisions up to maximum available SPS energies we suppose that the relevant time development stages of the relativistic nuclear collision comprise:

1. The pre-thermal stage lasting perhaps 0.2–0.4 fm/c, during which the thermalization of the initial quark-gluon distributions occur. During this time most of the entropy obtained in the collision must be created by mechanisms that are not yet understood — this is also alluded to as the period of de-coherence

of the quantum collision system. Our lack of understanding of this stage will not impact our results, as the reason that we lack in understanding is that the hadronic interactions erase the memory of this primordial stage, except for the entropy content.

2. The subsequent inter-penetration of the projectile and the target lasting about ~ 1.5 fm/c, probably also corresponding to the time required to reach chemical equilibrium of gluons g and light non-strange quarks u and d.

3. A third time period ($\simeq 5$ fm/c) during which the production and chemical equilibration of strange quarks takes place. During this stage many of the physical observables studied here will be initiated.

4. Hadronisation of the deconfined state ensues: it is believed that the fireball expands at constant specific entropy per baryon, and that during this evolution or at its end it decomposes into the final state hadrons, under certain conditions in an (explosive) process that does not allow for re-equilibration of the final state particles.

In the sudden hadronisation picture of the QGP fireball suggested by certain features seen in the analysis of the strange antibaryon abundances for the 200A GeV nuclear collision data,[4,14] the hadronic observables we study are not overly sensitive to the details of stage 4. Akin to the processes of direct emission, in which strange particles are made in recombination–fragmentation processes,[15,16] the chemical conditions prevailing in the deconfined phase are determining many relative final particle yields. Recent theoretical models show that such a sudden hadronisation may occur.[17] Furthermore if the hadronisation occurs as suggested by recent lattice results[1] at a relatively low temperature (e.g. 150 MeV), the total meson abundance which is determined by the entropy contents of the fireball at freeze-out of the particles, is found about 100% above the hadronic gas equilibrium expectations.[7] This is consistent with the source of these particles being the QGP.[4,5,7] The freeze-out entropy originates at early time in collision since aside of strangeness production which is responsible for about 10% additional entropy there is no significant entropy production after the initial state has occurred.[7]

The above remarks apply directly to the 200A GeV data. The general features of particle multiplicities obtained at 15A GeV are consistent with the thermal equilibrium hadronic gas state expectations.[18] However, the source of these particles could also be a QGP fireball, provided that a slow re-equilibration transition occurs under these conditions, leading to the equilibrium state among many final hadron gas particles.

The temperature of the fireball evolves in time and within our model we introduce here a few characteristic values which have both intuitive meaning and are useful in future considerations. We characterize the above described stages by the following temperatures:

T_{th} temperature associated with the initial thermal equilibrium,
$\downarrow$ *production of q, $\bar{q}$, G;*
T_{ch} temperature of chemical equilibrium for non-strange quarks and gluons,
$\downarrow$ *production of s, $\bar{s}$ quarks and fireball expansion;*
T_0 condition of maximal chemical equilibrium: 'visible' temperature,
$\downarrow$ *fireball expansion/particle radiation;*
$T_{f,s}$ temperature at freeze-out for non-strange or strange particles.

We encounter a considerable drop in temperature and obviously $T_{th} > T_{ch} > T_f$. However, the entropy content which determines the final particle multiplicities evolves more steadily, indeed it remains nearly constant: aside of the initial state entropy formation, in our model additional entropy increase is due to the formation of the strangeness flavor. Thus strangeness formation processes are acting like a viscosity slowing down the transverse flow of hadronic matter.

Initially, temperature decreases rapidly from T_{th} to T_{ch} since there is rapid quark and gluon production which establishes the chemical equilibrium, as we have shown[42] these processes generate little entropy. We will explicitly compute the values of T_{ch} for different systems balancing the energy per baryon and the collision pressure.

If the final state particles emerge directly, without re-equilibration, from the fireball,[14,15] this observed temperature $T_\perp$ in the particle spectra would be closely related to the full chemical equilibration temperature T_0 :

In the transverse mass spectra of strange (anti)baryons an inverse temperature slope $T_\perp$ ($= 232 \pm 5$ MeV in S–A collisions at 200A GeV) is found, and the important matter is to relate this observed value to the initial T_{ch} condition of the fireball. It is to this end that we have introduced above the quantity T_0 which arises from T_{ch} when we relax strangeness to (nearly) full chemical equilibrium, keeping the entropy content of gluons and light flavor unchanged. T_0 is always somewhat smaller than T_{ch} since energy has been spend to produce strangeness.[13] Even more energy is spend into the expansion and thus the temperature at freeze out is certainly considerably lower than T_0. When the final state particles emerge from the flowing surface, they are blue-shifted by the flow velocity. This Doppler shift effect restores the high apparent $T_\perp$ in high $m_\perp$ particle spectra:[19]

$$T_\perp \simeq \sqrt{\frac{1+v_f}{1-v_f}} T_f \,, \tag{7}$$

and $T_\perp$ is found in model calculations to be close if not exactly equal to the value T_0 that would be present in the chemically equilibrated fireball, provided that no reheating has occured in a strong phase transition of first order. Despite our still considerable ignorance of the dynamics of fireball and particle freeze-out mechanisms and conditions, we think that the uncertainty in the value of the temperature T_0 as derived from the value of $T_\perp$ is not large. Namely, if QGP phase is directly dissociating by particle emission, this is trivially so, since we see what happened in a direct observation. If, as is generally assumed, there were to be substantial flow, one can assume some temperature T_0, and given equations of state (EoS), obtain the

hydrodynamic radial expansion;[20] especially at the high $m_\perp \simeq 2$ GeV the resulting inverse slope temperature $T_\perp$ of the particle is found smaller but almost equal to T_0.

3 Experimental Methods and Results

Only recently experimental results have been presented which lead to a comprehensive examination of our ideas and results.[2] These reports address in detail results regarding the overall enhancement of strange particle yields seen at 15 and 200A GeV, and in particular the observed enhancement in the yield of multi-strange antibaryons in comparison to expectations based on the experimental study of N–N and N–A collisions at comparable energy. As we shall describe, our analysis of the data is in full agreement with these results both for the results obtained at 160/200A GeV and at the 15A GeV collisions. However, the lower energy data suggest a more complex final state behavior that makes the interpretation of these results ambiguous. We will focus in this report our attention on the sudden hadronisation and the SPS results.

'Strangeness' is a very informative observable of dense hadronic matter. Note that spectra of several strange particles $K^\pm$, K_S, ϕ, $\bar{p}$, Λ, $\overline{\Lambda}$, Ξ^-, $\overline{\Xi^-}$, Ω, $\overline{\Omega}$ are studied as function of rapidity and transverse mass. We have included in above list the closely related antiprotons $\bar{p}$, which are also fully made in the collision. The classic observables based on these particles are their abundance ratios: leaving out an overall normalization factor associated with the reaction volume, and recalling that there are relations between the abundances such as of kaons ($K^+ + K^- \simeq 2K_S$) we have 9 independent normalization parameters describing the yields of $K^\pm$, K_S, ϕ, $\bar{p}$, Λ, $\overline{\Lambda}$, Ξ^-, $\overline{\Xi^-}$, Ω, $\overline{\Omega}$. These can be redundantly measured with the help of the $36 = 9 \cdot 8/2$ independent particle yield ratios. Aside of the yield normalization parameters, there are in principle 11 different spectral shapes which we presume to be closely related to each other and to be governed by the same inverse slope parameter (temperature) parameter. The experimental fact that once effects related to particle decays and matter expansion (transverse flow) are accounted for, the $m_\perp$ spectra of all these particles are characterized by a common temperature, cannot be taken lightly and suggest strongly that the source of all strange particles is indeed thermalized with a common temperature T and that a common mechanism governs production of the very different strange particles, as well as $\bar{p}$.

3.1 Strange Particles

Among strange baryons (and antibaryons) we record:

HYPERONS $Y(qqs)$ and $\overline{Y}(\bar{q}\bar{q}\bar{s})$ comprising two types of particles[b], the isosinglet Λ and the isotriplet Σ.

• The isospin singlet lambda $\Lambda(uds)$, a neutral particle of mass 1.116 GeV that decays weakly with proper path length $c\tau = 7.9$ cm. The dominant and commonly observed

---

[b]Here and below the valence quark content is indicated in parenthesis
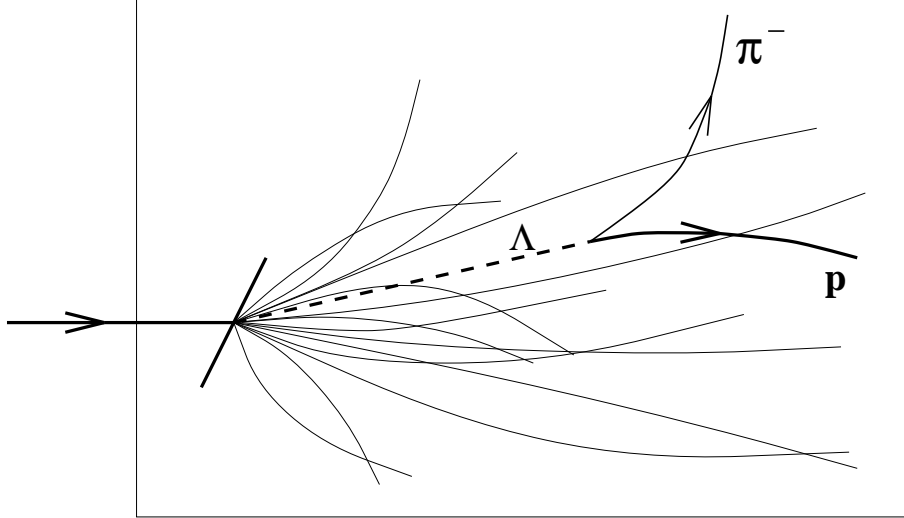
Figure 1: Schematic representation of the Λ-decay topological structure showing as dashed line the invisible Λ and the decay 'V' of the final state charged particles. Other directly produced charged particle tracks propagating in a magnetic field normal to the figure plane are also shown.

decay is

$$\Lambda \to p + \pi^- \quad (64\%),$$

the other important weak decay

$$\Lambda \to n + \pi^0 \quad (36\%)$$

has only the hard to identify neutral particles in the final state. The decay of a neutral particle into a pair of charged particles forms a characteristic 'V' structure shown in Fig. 1. Aside of the ground state (positive parity, spin $1/2$) we encounter a spin $1/2^-$ resonance Λ (1.405) and also $3/2^-$ state Λ (1.520). These and higher excited resonance states (13 are presently known with mass below 2.350 GeV) decay hadronically with the two principle channels:

$$\begin{aligned} \Lambda^* &\to \text{Y} + \text{meson(s)}\,, \\ \Lambda^* &\to \text{N} + \overline{\text{K}}\,. \end{aligned}$$

Since the hadronic decays have free space proper decay paths of 1–10 fm (widths $\Gamma = 16$–250 MeV), all these resonances contribute to the abundance of the observed 'stable' strange particles Λ, K. The practical approach to the observation of Λ is to observe the (dominant) decay channel with two final state charged particles pointing to a formation vertex remote from the collision vertex of projectile and target. This approach includes in certain kinematic region the events which originate from the K_S decay (see below). The well established method of data analysis has been reviewed elsewhere.[21]

• The isospin triplet Σ^0, $\Sigma^\pm$ of mass 1.189 GeV. The decay of neutral

$$\Sigma^0 \to \Lambda + \gamma + 76.9 \text{ MeV}$$

occurs within $c\tau = 2.22\ 10^{-9}$ cm, thus well away from the reaction region, but for the observer in the laboratory this remains indistinguishable from the interaction vertex. Consequently all measurements of Λ combine the abundances of Λ and Σ^0, and all the higher resonances that decay hadronically into Σ^0. Σ^0 is taken to be produced with a thermally reduced rate compared to the abundance of Λ:

$$N_{\Sigma^0} = \left(\frac{m_\Sigma}{m_\Lambda}\right)^a e^{-(m_\Sigma - m_\Lambda)/T} N_\Lambda. \tag{8}$$

Here the power a depends what precisely is measured. For example when N stands for $E d^3 N/dp^3$ we have $a = 1$; when this spectral distribution is integrated over a wide region of rapidity, N stands for $dN/dM_\perp$ and we find $a = 3/2$ since we have $m/T >> 1$ ($a = 0$ follows when $m/T << 1$).

As with Λ there are several (nine) heavier Σ resonances known at $m \le 2.250$ GeV. When produced, they all decay hadronically producing $\overline{K}, \Lambda, \Sigma$.

Turning briefly to the charged $\Sigma^\pm$ we note that there is only one dominant decay channel for the Σ^- decay:

$$\Sigma^- \to n + \pi^- \qquad c\tau = 4.43 \text{ cm}.$$

Because there are two isospin allowed decay channels of similar strength for the Σ^+:

$$\begin{aligned}
\Sigma^+ &\to p + \pi^0 & 51.6\% \\
&\to n + \pi^+ & 48.3\%
\end{aligned}$$

the decay path here is nearly half as long, $c\tau = 2.4$ cm. $\Sigma^\pm$ have not yet been studied in the context of QGP studies, as they are relatively more difficult to observe compared to Λ — akin to the Ξ decay (see below) there is always an unobserved neutral particle in the final state, but unlike Ξ the kink that is generated by the conversion of one charged particle into another, accompanied by the emission of a neutral particle, is not associated with subsequent decay of the invisible neutral particle accompanied by a 'V' charged particle pair.

It is generally subsumed that abundances of all three Σ are equal.

CASCADES $\Xi(qss)$ and $\overline{\Xi}(\bar{q}\bar{s}\bar{s})$
The double strange cascade baryons and antibaryons $\Xi^0(ssu)$ and $\Xi^-(ssd)$ are below the mass threshold for hadronic decays into hyperons and kaons, also just below the weak decay threshold for $\pi + \Sigma$ final state. Consequently we have one primary decay in each case:

$$\begin{aligned}
\Xi^-(1321) &\to \Lambda + \pi^- & c\tau = 4.9 \text{ cm}, \\
\Xi^0(1315) &\to \Lambda + \pi^0 & c\tau = 8.7 \text{ cm}.
\end{aligned}$$
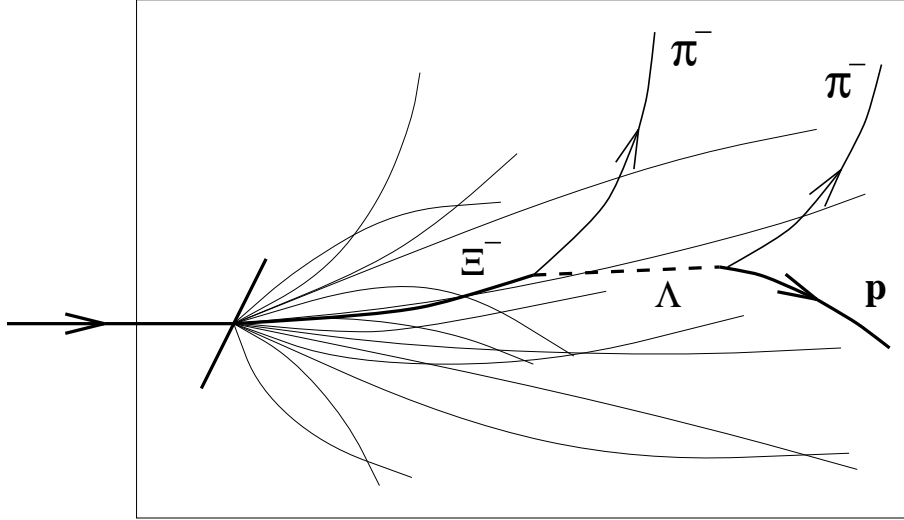
Figure 2: Schematic representation of the Ξ^--decay topological structure showing as dashed line the invisible Λ emerging from the decay kink and the decay 'V' of the final state charged particles. Other directly produced charged particle tracks propagating in a magnetic field normal to the figure plane are also shown.

The first of these reactions can be found in charged particle tracks since it involves conversion of the charged Ξ^- into the charged π^-, with the invisible Λ carrying the 'kink' momentum. For Ξ^- to be positively identified it is required that the kink combines properly with an observed 'V' of two charged particles which identify a Λ decay. This decay topology situation is illustrated in Fig. 2.

There are also several Ξ^* resonances known, which (with one exception) feed down into the hyperon and kaon abundances by weak decays. The exception is the hadronic decay of the spin-3/2 recurrence of the spin-1/2 ground state:

$$\Xi(1530) \ \rightarrow \ \Xi + \pi \qquad \Gamma = 9.5\,\mathrm{MeV}\,.$$

Since the 3/2 state is populated twice as often as is the spin 1/2 ground state, the penalty due to the greater mass is almost compensated by the statistical factor, in particular should the source of these particles be at high (that is $T > 180$ MeV) temperatures.

OMEGAS $\Omega(sss)^-$ and $\overline{\Omega}(\bar{s}\bar{s}\bar{s})$
There are several primary weak interaction decay channels leading to the relatively short proper decay path $c\tau = 2.46$ cm:

$$
\begin{aligned}
\Omega(1672)^- \ &\rightarrow \ \Lambda + \mathrm{K}^- & 68\%\,, \\
&\rightarrow \ \Xi^0 + \pi^- & 24\%\,, \\
&\rightarrow \ \Xi^- + \pi^0 & 9\%\,.
\end{aligned}
$$

The first of these decay channels is akin to the decay of the Ξ^-, except that the pion is now a kaon. In the other two options, after cascading has finished, there is a neutral pion in the final state, which makes the detection of these channels not practical. There is only one known, rather heavy, $\Omega^*(2250)$ resonance.

It should be remembered that the abundance of Ω benefits from the spin-3/2 statistical factor.

KAONS $K(q\bar{s})$, $\overline{K}(\bar{q}s)$

● **neutral kaons** K_S, K_L

This is not the place to describe in detail the interesting physics of the short and long lived neutral kaons, except to note that both are orthogonal combinations of the two neutral states $(d\bar{s})$, $(\bar{d}s)$. The short lived combination has a $c\tau = 2.676$ cm and can be observed in its charged decay channel:

$$
\begin{aligned}
K_S &\rightarrow \pi^+ + \pi^- & 69\%\,, \\
&\rightarrow \pi^0 + \pi^0 & 31\%\,.
\end{aligned}
$$

Care must be exercised to separate the K_S decay from Λ decay, since in both cases there are two a priori not identified charged particles in the final state, making a 'V' originating in an invisible neutral particle.

The long lived kaon K_L with $c\tau = 1549$ cm has not been studied in relativistic heavy ion collision experiments.

● **charged kaons** $K^+(u\bar{s})$, $K^-(\bar{q}s) = \overline{K}^+$
Charged kaons can be observed directly since their mass differs sufficiently from the lighter $\pi^\pm$ and the heavier proton/antiproton. However, at the SPS energies the CM-frame has rapidity 2.5–3 and thus the distinction between the different charged particles is not easy, though not impossible, such that directly measured spectra should become available in the near future. $K^\pm(494)$ decay with $c\tau = 371$ cm, with three dominant channels, of which the one with only charged particles in final state (smallest branching ratio) has been used in our field:

$$
\begin{aligned}
K^+ &\rightarrow \mu^+ + \nu_\mu & 63.5\%\,, \\
&\rightarrow \pi^+ + \pi^0 & 21.2\%\,, \\
&\rightarrow \pi^+ + \pi^+ + \pi^- & 5.6\%\,.
\end{aligned}
$$

In general it is subsumed that the mean abundance of the charged kaons is similar to the abundance of the neutral K_S.

ϕ-**MESON** $\phi(s\bar{s})$
The vector meson ϕ with mass 1019.4 MeV has a relatively narrow full width $\Gamma_\phi = 4.43$ MeV, since it is barely above the threshold for the decay into two kaons. Consequently, the total width and thus particle yield could be easily influenced by hadronic
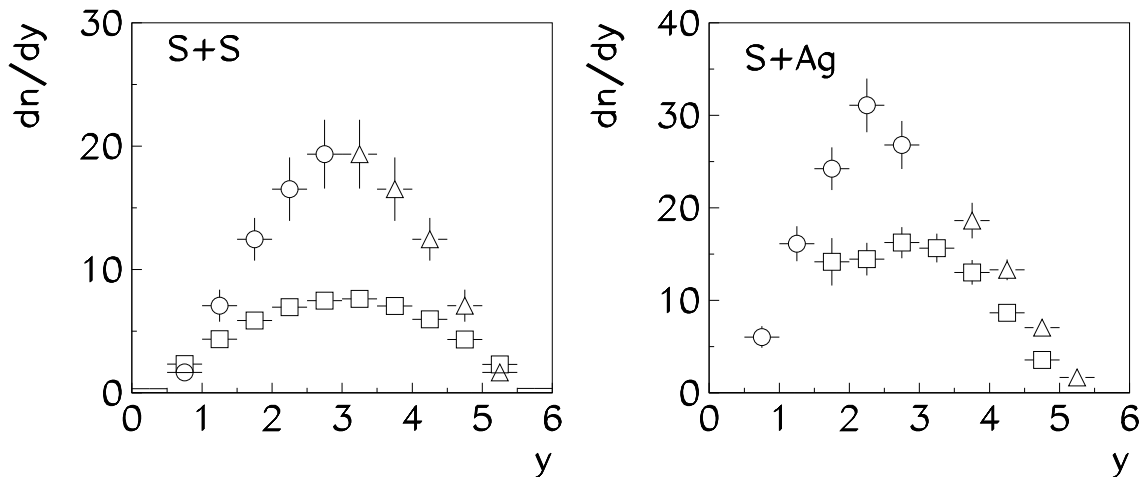
Figure 3: Abundance of $1.6\Lambda + 4K_S + 1.6\overline{\Lambda}$ as function of rapidity. On the left S–S, on the right S–Ag (open circles are the directly measured data). The triangles are reflected data points for S–S and reflected-interpolated data employing S–S and S–Ag. The squares in S–S case are the results for N–N collisions scaled up by the pion multiplicity ratio, for S–Ag these are the scaled up p–S results. Courtesy of NA35 collaboration.[22]

medium effects: these could facilitate induced decays. On the other hand the slow decays into two leptons

$$
\begin{aligned}
\phi \;&\to\; e^+ + e^- \qquad 0.031\% \,, \\
&\to\; \mu^+ + \mu^- \qquad 0.025\% \,,
\end{aligned}
$$

which have partial widths 1.37 keV and 1.1 keV allow the determination of the number of ϕ-mesons that emerge from the interaction region. While absolute particle yields may be difficult to determine, one can compare the yield of ϕ to the yield of $\rho(770)$-meson, the $(q\bar{q})$ partner of the ϕ.

3.2 Experimental Results

We now briefly describe the key experimental results on which our here presented theoretical developments are based either in detail or/and conceptual design:

● **Centrality of strangeness production**
We consider a measure of the abundance of $\langle s + \bar{s} \rangle$ in Fig. 3. We show here the integrated transverse mass $m_\perp = \sqrt{m^2 + p_\perp^2}$ distribution for $1.6\Lambda + 4K_S + 1.6\overline{\Lambda}$ as determined by the experiment NA35,[22] as function of rapidity. For the case of S–S the open circles are the measured data points, the open triangles are the symmetrically reflected data points, and squares are the results of N–N (isospin symmetric nucleon-nucleon) collisions scaled up by pion multiplicity; the difference, most pronounced at central rapidity $y \simeq 3$ shows a new source of strangeness in the collision, and the important lesson to be drawn from this result is that strangeness enhancement

14

originates in the central rapidity region. We also show in Fig. 3 similar results for S–Ag collisions: here the open circles are the measured points, open triangles are estimates based on S–S and the 'reflected' S–Ag results, and the open squares are pion multiplicity scaled p–S results.

• Anomalies of strange antibaryon abundances

The WA85 collaboration has extensively studied in the central rapidity region the relative abundance of the different strange baryons and antibaryons. The particle spectra ratios have been obtained at $p_\perp \geq 1$ GeV. The results for relative abundances can be presented both for the sum of abundance with $p_\perp \geq 1$ GeV or using as cut a fixed value $m_\perp \geq 1.7$ GeV. In the thermal model this latter set of values is of primary interest. However, given prior studies of relative particle abundances one often identifies the anomalies using the fixed $p_\perp$ approach. Moreover such ratios correspond more closely to the total particle abundance ratio, as we shall see in section 8.

In the thermal fireball model the particle yields can be connected to the physical properties of the fireball. The ratios of strange antibaryons to strange baryons *of same particle type* at fixed $m_\perp$:

$$R_\Lambda = \overline{\Lambda}/\Lambda|_{m_\perp}, \quad R_\Xi = \overline{\Xi}/\Xi|_{m_\perp} \quad \text{and} \quad R_\Omega = \overline{\Omega}/\Omega|_{m_\perp},$$

are in our approach simple functions of the quark fugacities. For the available two ratios in experiment WA85 one has specifically

$$R_\Xi = \frac{\overline{\Xi^-}}{\Xi^-} = \frac{\lambda_d^{-1}\lambda_s^{-2}}{\lambda_d\lambda_s^2}, \qquad R_\Lambda = \frac{\overline{\Lambda}}{\Lambda} = \frac{\lambda_d^{-1}\lambda_u^{-1}\lambda_s^{-1}}{\lambda_d\lambda_u\lambda_s}. \tag{9}$$

These ratios can easily be related to each other, in a way which shows explicitly the respective isospin asymmetry factors and strangeness fugacity dependence. Eq. (9) implies:

$$R_\Lambda R_\Xi^{-2} = e^{6\mu_s/T} \cdot e^{2\delta\mu/T}, \qquad R_\Xi R_\Lambda^{-2} = e^{6\mu_q/T} \cdot e^{-\delta\mu/T}. \tag{10}$$

Eq. (10) is generally valid, irrespective of the state of the system (HG or QGP), as long as the momentum spectra of the radiated particles are 'thermal' with a common temperature (inverse slope). We see that once the left hand side is known experimentally, it determines rather accurately the values of μ_q, μ_s which enter on the right hand side with a dominating factor 6, while the (small) isospin asymmetry $\delta\mu$ plays only a minor, but significant role, given the precision of the experimental results.[4] This explains how, by applying these identities to the early WA85 data,[23] it has been possible[24] to determine the chemical potentials with considerable precision in spite of the still relatively large experimental errors on the measured values of R_Λ, R_Ξ. The more precise results:

$$\begin{aligned} R_\Lambda &= 0.20 \pm 0.01 \\ & \qquad\qquad\qquad\qquad \text{for } y \in (2.3, 2.8) \text{ and } m_\perp > 1.9 \text{ GeV.} \\ R_\Xi &= 0.41 \pm 0.05 \end{aligned} \tag{11}$$

have been analyzed carefully in our recent work.[4,14] We obtain the following values of the chemical potentials for S–W central collisions at 200A GeV:

$$\frac{\mu_q}{T} = \frac{\ln R_\Xi/R_\Lambda^2}{5.94} = 0.39 \pm 0.04 \,, \tag{12}$$

$$\frac{\delta\mu}{T} = \frac{\mu_q}{T}(R_f - 1) = 0.031 \pm 0.003 \,, \tag{13}$$

$$\frac{\mu_s}{T} = \frac{\ln R_\Lambda/R_\Xi^2 \; - 0.062}{6} = 0.02 \pm 0.05 \,. \tag{14}$$

Here R_f is valence quark flavor asymmetry:

$$R_f = \frac{\langle d - \bar{d} \rangle}{\langle u - \bar{u} \rangle} \,. \tag{15}$$

and its value is $R_f = 1.08$ for S–W/Pb and $R_f = 1.15$ for Pb–Pb. For the QGP thermal fireball with $\mu_q < \pi T$ one finds[24]

$$R_f^{\mathrm{QGP}} \simeq \frac{\mu_d}{\mu_u} \simeq 1 + \frac{\delta\mu}{\mu_q} \,. \tag{16}$$

In view of our current work[25,26] which allows to determine the value of λ_q reached in the collision, we have been able to explain these particle ratios and will discuss in section 8 below the behavior of these ratios as function of energy.

Strangeness phase space saturation is probed when ratio of particles is considered that contains a different number of strange quarks. In Fig. 4 such a World sample of strange baryon and antibaryon data is presented. We note the strong enhancement of the ratios seen in heavy ion reactions (S–S/W at 200A GeV).

We now show how in the thermal model the ratios between antibaryons with different strange quark content are dependent on the degree of the strangeness saturation. Up to cascading corrections a complete cancelation of the fugacity and Boltzmann factors occurs when we form the product of the abundances of baryons and antibaryons, comparing this product for two different particle kinds,[14] e.g.,

$$\left. \frac{\Xi^-}{\Lambda} \cdot \frac{\overline{\Xi^-}}{\overline{\Lambda}} \right|_{m_\perp > m_\perp^{\mathrm{cut}}} = \gamma_s^2 \,, \tag{17}$$

where we neglected resonance feed-down contribution in first approximation. Similarly we have

$$\gamma_s^2 = \left. \frac{\Lambda}{p} \cdot \frac{\overline{\Lambda}}{\overline{p}} \right|_{m_\perp > m_\perp^{\mathrm{cut}}} = \left. \frac{\Omega^-}{2\Xi^-} \cdot \frac{\overline{\Omega^-}}{2\overline{\Xi^-}} \right|_{m_\perp > m_\perp^{\mathrm{cut}}} \,, \tag{18}$$

where in the last relation the factors 2 in the denominator correct for the spin-3/2 nature of the Ω.

16
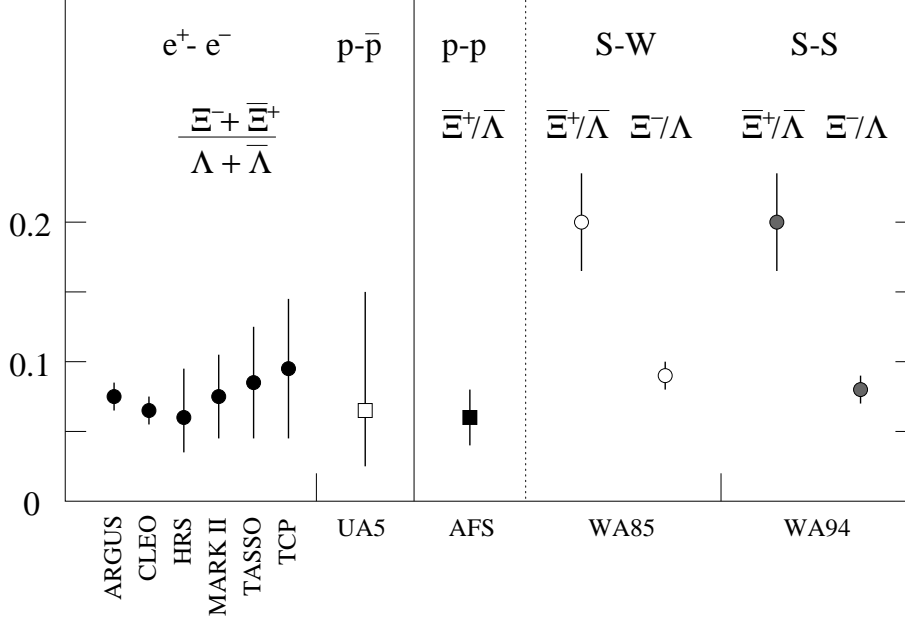
Figure 4: Ratio (at fixed $p_\perp$) of (multi)strange baryon-antibaryon particle abundance, measured in the central rapidity region at 200A GeV S–S/W collisions, compared to ratios obtained in lepton and nucleon induced reactions. Data assembled by the WA85/94 collaboration.[23]

We note that in the kinematic domain of Eqs. (11) the experimental results reported by the WA85 collaboration are:

$$\frac{\overline{\Xi^-}}{\overline{\Lambda + \Sigma^0}} = 0.4 \pm 0.04\,, \quad \frac{\Xi^-}{\Lambda + \Sigma^0} = 0.19 \pm 0.01\,. \tag{19}$$

If the mass difference between Λ and Σ^0 is neglected, this implies in the framework of the thermal model that an equal number of Λ's and Σ^0's are produced, such that

$$\frac{\overline{\Xi^-}}{\overline{\Lambda}} = 0.8 \pm 0.08\,, \qquad \frac{\Xi^-}{\Lambda} = 0.38 \pm 0.02\,. \tag{20}$$

The fact that the more massive and stranger anticascade practically equals at fixed $m_\perp$ the abundance of the antilambda is most striking. These results are inexplicable in terms of hadron-cascade models for the heavy-ion collision.[27] The relative yield of $\overline{\Xi^-}$ is 3.5 times greater than seen in the p–p ISR experiment[28] and all other values reported in the literature, which amounts to a 4 s.d. effect.[23] Combining the experimental result Eq. (20) with Eqs. (17), we find the value $\gamma_s = 0.55 \pm 0.04$. In a full analysis[4] which accounts more precisely for resonance decay and flow, this result becomes

$$\gamma_s = 0.75 \pm 0.15\,. \tag{21}$$

Another most remarkable result related to these findings is due to the NA35 collaboration:[29] in Fig. 5 we show the ratio of the rapidity density dn/dy at central
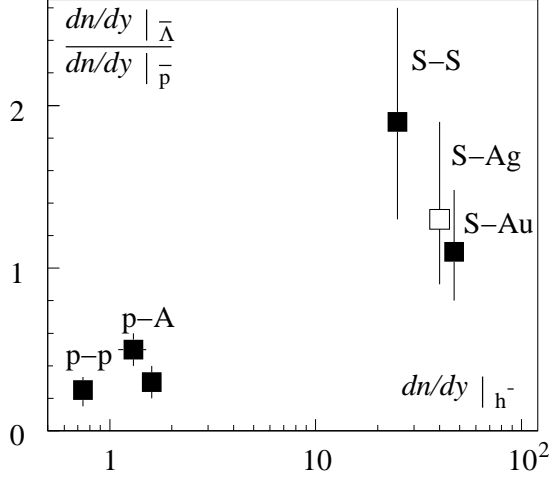
Figure 5: Ratio of the rapidity density dn/dy for $\overline{\Lambda}/\bar{p}$, measured at central y, as function of the negative hadron central rapidity density $dn/dy|_{h^-}$. Courtesy of NA35 collaboration.[29]
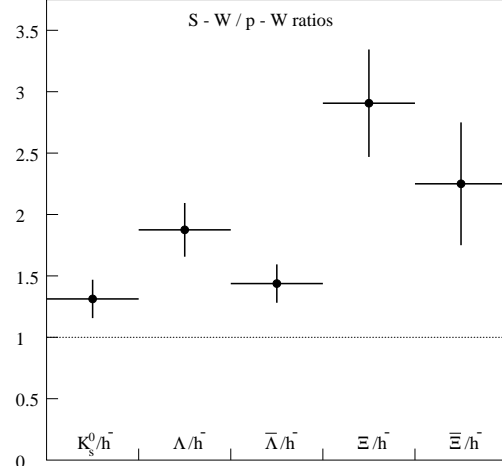
Figure 6: Ratio of h^- normalized particle abundances: S–W results divided by p–W results at 200A GeV in the same rapidity window near to $2.5 < y < 3$. Dotted line: expected yields. Courtesy of WA85 collaboration.[23]

y of $\overline{\Lambda}/\bar{p}$, as function of the negative hadron central rapidity density $dn/dy|_{h^-}$. The p–p and p–A reactions are at small values of $dn/dy|_{h^-}$, while the S–S, S–Ag, S–Au reactions are accompanied by a relatively high $dn/dy|_{h^-}$. We observe that there is an increase in this ration by nearly factor 5, and even more significantly, the abundance of the *heavier* and *strange* $\overline{\Lambda}$ is similar if not greater than the abundance of $\bar{p}$.

• **Collectivity of strange particle production**

The WA85 collaboration[23] has shown that there is a trend in these anomalous strange baryon abundances in that the yields in nuclear collision S–W (normalized by h^- abundance) when compared to the p–W collisions are increasing with the strangeness content, as illustrated in Fig. 6. This indicates that strange particles are formed in some collective mechanism, which favors the assembly of multiply strange hadrons. Comparable result is reported by the NA38 collaboration[31] which has shown that the ratio of

$$\frac{\phi}{\rho + \omega} \propto \frac{s\bar{s}}{q\bar{q}}$$

rises by nearly a factor three in S–U compared to p-W reactions, in collisions involving greatest particle density.

• **Thermal nature of (strange) particle spectra**

The central rapidity WA85[30] transverse mass spectra $m_\perp^{-3/2} dN_i/dm_\perp$ of diverse strange particles are shown in the Fig. 7. It is striking that within the observed interval $1.5 < m_\perp < 2.6$ GeV the particle spectra are exponential, as required in the thermal fireball comprising longitudinal collision flow. Even more significantly, there is clearly a common inverse slope temperature, with its inverse value around $T = 232$ MeV. It
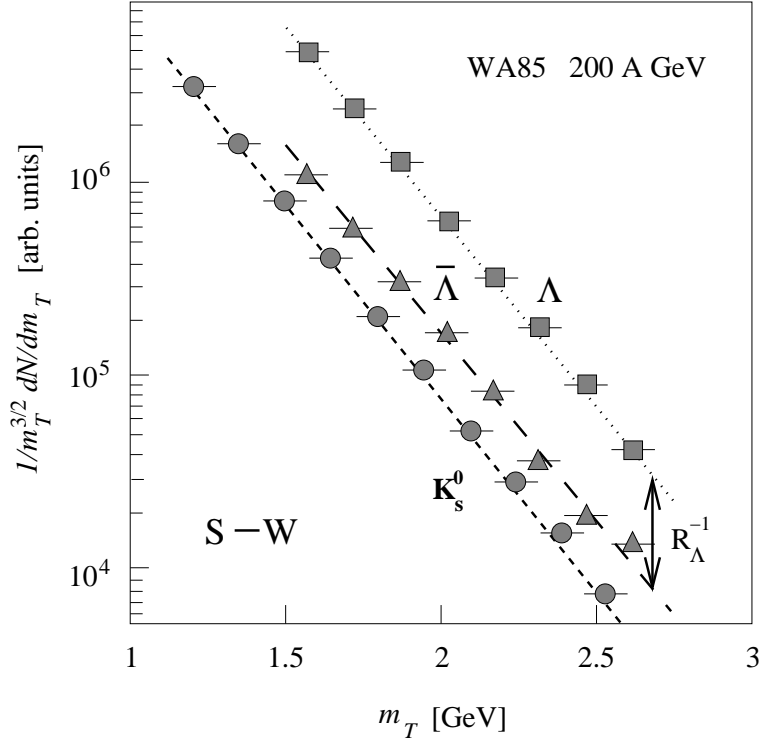
Figure 7: Strange particle spectra for Λ, $\overline{\Lambda}$, K_s . Line connecting the Λ and $\overline{\Lambda}$ spectra, denoted R_Λ^{-1}, shows how the ratio R_Λ of these particle abundances can be extracted. Experimental WA85 results from reference.[30]

is remarkable that for this $m_\perp$ range the WA80 collaboration[32] obtained data in S–Au collisions for the neutral hadrons π^0, η which is consistent. In Fig. 8 we have replotted the WA80 results multiplying the invariant cross sections by the power $m_\perp^{-1/2}$, so that there is direct correspondence between the data of experiments[c] WA85 and WA80, both experiments focus on the central region in rapidity $2.1 < y < 2.9$. Similar results were also obtained by the NA35 collaboration[33] and these temperatures are consistent with the results considered here. The upper straight line in Fig. 8 corresponds to an eye-ball thermal fit (emphasized in the WA85 $m_\perp$-interval $1.5 < m_\perp < 2.5$ GeV), with $T = 232$ MeV for the S–Ag system, the lower solid line is for S–S collisions and was done with $T = 210$ MeV. The choice of S–S temperature was based on the WA94[23] results for spectra of strange antibaryons. Note that we separated by factor 0.4 the π^0 S–S results from the S–Au results; and that the relative η to π^0 normalization enhancement is 2.5, which factors makes the η abundance fall onto the π^0 yields. It is noteworthy that the WA80 particle spectra span 7 decades. The rise in meson

---

[c]The pre-exponential factor is $m_\perp^{-3/2}$, instead of $m_\perp^{-1}$, because the sum of the rapidity coverage window $\Delta y_{\mathrm{w}} \simeq 0.8$ and longitudinal flow $\Delta y_{\mathrm{fl}} \simeq 1$ is almost as large as the full rapidity width of the particle spectra, which effect induces even at central rapidity the shape expected for rapidity-integrated $m_\perp$ spectra.
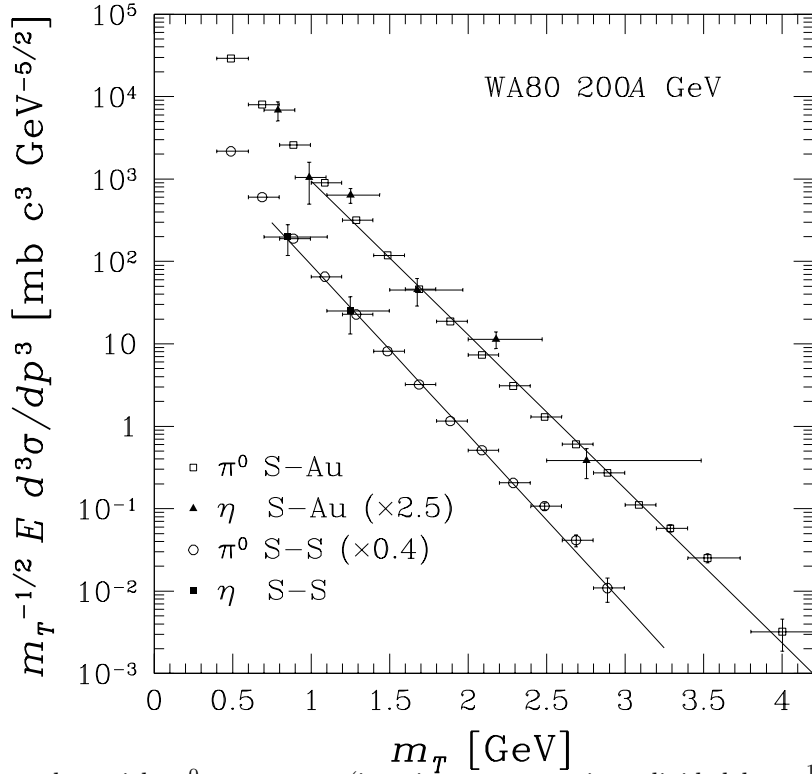
Figure 8: Neutral particle π^0, η spectra (invariant cross sections divided by $m_\perp^{1/2}$) in central rapidity interval $2.1 < y < 2.9$. Upper solid line S–Au: thermal spectrum with temperatures $T = 232$ MeV; lower solid line S–S: $T = 210$ MeV. Experimental data courtesy of the WA80 collaboration.[32]

yield at low $m_\perp$ is due to the here unaccounted contribution of decaying resonances produced very abundantly in the thermal model. Similarly, some of the concavity of the spectrum arises from non-trivial and in the current approach unaccounted flow effects.

4 Thermal QGP Fireball

The QGP equations of state are of considerable relevance for the understanding of the magnitudes of different variables we consider here. We use a rather standard, perturbative/nonperturbative QCD improved set of relations based on the Fermi/Bose liquid model with thermal particle masses. The partition function of the interacting quark-gluon phase can be written as:

$$\ln Z^{\mathrm{QGP}} = \sum_{i \in \mathrm{QGP}} \frac{g_i(\alpha_s)V}{2\pi^2} \int \pm \ln\left(1 \pm \gamma_i \lambda_i e^{-\sqrt{m_i^2(T)+p^2}/T}\right) p^2\, dp\,, \qquad (22)$$

20

where $i = G$, q, $\bar{q}$, s, $\bar{s}$, with $\lambda_{\bar{i}} = \lambda_i^{-1}$ and $\gamma_{\bar{i}} = \gamma_i$. We take into account the QCD interactions between quarks and gluons by allowing for thermal masses

$$m_i^2(T) = (m_i^0)^2 + (c\,T)^2\,. \tag{23}$$

For the current quark and gluon masses we take:

$$m_{\rm q}^0 = 5\ \text{MeV}, \quad m_{\rm s}^0 = 160\ \text{MeV}, \quad m_{\rm g}^0 = 0\,.$$

We have $c^2 \propto \alpha_{\rm s}$, α_s being the QCD coupling constant. We fix $c = 2$, arising for $\alpha_s \sim 1$, while also allowing for another effect of the QCD-interactions, the reduction of the number of effectively available degrees of freedom: we implement the following effective counting of gluon and quark degrees of freedom, motivated by the perturbative QCD formulæ

$$
\begin{aligned}
g_{\rm g} = 16 &\quad\rightarrow\quad g_{\rm g}(\alpha_s) = 16\left(1 - \frac{15\alpha_s}{4\pi}\right), \\
g_{i-{\rm T}} = 6 &\quad\rightarrow\quad g_{i-{\rm T}}(\alpha_s) = 6\left(1 - \frac{50\alpha_s}{21\pi}\right), \\
g_{i-{\rm B}} = 6 &\quad\rightarrow\quad g_{i-{\rm B}}(\alpha_s) = 6\left(1 - 2\frac{\alpha_s}{\pi}\right),
\end{aligned}
\tag{24}
$$

where $i = u$, d, s. In Eq. (24) two factors are needed for quarks: the factor $g_{i-{\rm T}}$ controls the expression when all chemical potentials vanish (the T^4 term in the partition function for massless quarks) while $g_{i-{\rm B}}$ is taken as coefficient of the additional terms which arise in presence of chemical potentials. We took $\alpha_s = 0.6$ which turned out to be the value best suited for the experimental data points.

We begin the study of the physical properties of the QGP fireball by considering the constraint between T and $\lambda_{\rm q}$ arising from a given initial specific energy content[d] E/B. The collision energy gives us the values of the constraints to consider

$$\frac{E}{B} = \frac{\eta_{\rm E} E_{\rm CM}}{\eta_{\rm B} A_{\rm part}} \simeq \frac{E_{\rm CM}}{A_{\rm part}}, \tag{25}$$

where $\eta_{\rm E}$ and $\eta_{\rm B}$ are respectively the stopping fraction[9] of energy and baryonic number and $A_{\rm part}$ is the number of nucleons participating in the reaction. The last equality follows when the stopping fractions are equal — the experimental particle spectra we are addressing here, and in particular the visible presence of baryons in the central rapidity region, are implying that this is a reasonable assumption for the current experimental domain. In consequence, the energy per baryon in the fireball is to be taken as being equal to the kinematic energy available in the collision. In the current laboratory target experiments we have the following kinematic energy content:

---

[d]Here B is the baryon number. To avoid confusion, below the bag constant is denoted $\mathcal{B}$.
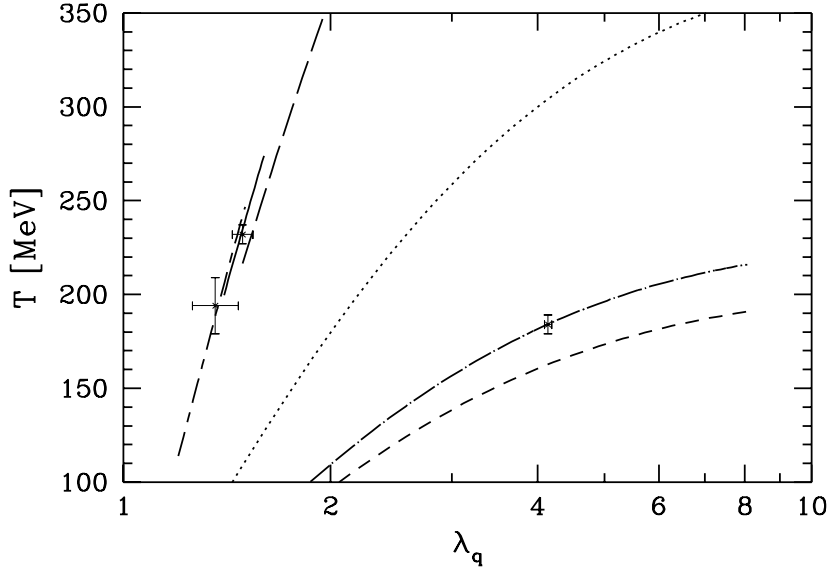
Figure 9: QGP-EoS constraint between temperature T and light quark fugacity λ_q for a given fireball energy content per baryon E/B appropriate for the AGS and SPS collision systems. Left to right: 2.3 (Au–Au), 2.6 (Si–Au), 4.3 (A–A), 8.6 (Pb–Pb), 8.8 (S–PB/W) and 9.6 (S–S) GeV. See text for a discussion of experimental point.

$$
\begin{aligned}
\text{Au–Au at 10.5A GeV} &\quad \rightarrow \quad E/B = 2.3 \text{ GeV},\\
\text{Si–Au at 14.6A GeV} &\quad \rightarrow \quad E/B = 2.6 \text{ GeV},\\
\text{A–A at 40A GeV} &\quad \rightarrow \quad E/B = 4.3 \text{ GeV},\\
\text{Pb–Pb at 158A GeV} &\quad \rightarrow \quad E/B = 8.6 \text{ GeV},\\
\text{S–W/Pb at 200A GeV} &\quad \rightarrow \quad E/B = 8.8 \text{ GeV},\\
\text{S–S at 200A GeV} &\quad \rightarrow \quad E/B = 9.6 \text{ GeV}.
\end{aligned}
$$

Note that above we assumed collision with the geometric target tube of matter[11] when the projectile is smaller than the target. In Fig. 9 we show in the T–λ_q plane the lines corresponding to this constraint on the QGP-EoS. In the middle the line corresponding to the lowest SPS accessible energy, 4.3 GeV, is depicted, which bridges the current SPS domain shown to the left to the BNL region on the lower right. The experimental crosses show the values of λ_q arising in our data analysis,[4, 5, 18] combined with the inverse slopes temperatures, extracted from transverse mass particle spectra. The fact that the experimental results fall on the lines shown in Fig. 9 is primarily due to the choice $\alpha_s = 0.6$ — as this is the usual value in this regime of energy it implies for a QGP fireball EoS hypothesis that the assumption that stopping of energy and baryon number is similar deserves further consideration.

There now remains the issue what physical constraint or principle determines which of the possible pair of T, λ_q values along the individual curves depicted in Fig. 9 is experimentally recorded by the cross shown. We have explored the properties of the QGP phase along these lines of constant energy per baryon and have noticed that with increasing T the pressure in the QGP phase increases, and that the experimental points coincide with the dynamical pressure generated in the collision. This gives
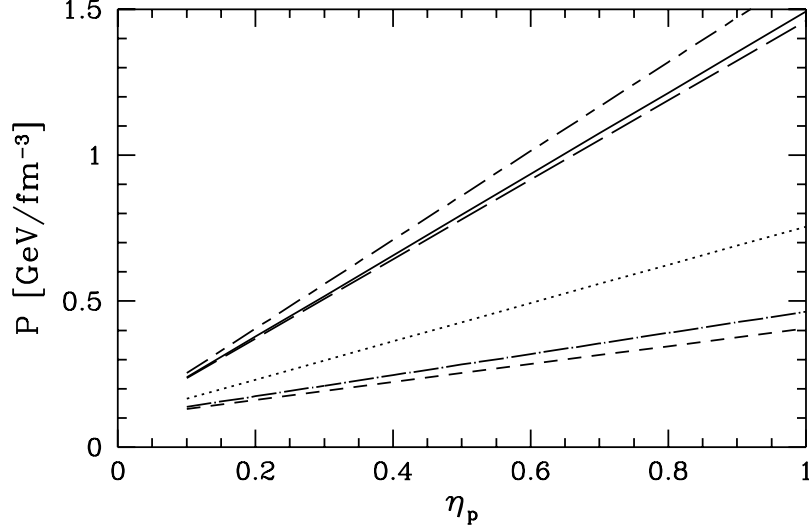
Figure 10: The collision pressure P as function of momentum stopping η_{p} for different values of E/B — 2.3, 2.6, 4.3, 8.6, 8.8 and 9.6 GeV (from bottom to top, solid line is for 8.8 GeV).

birth to the intuitive idea that the initial conditions reached in the central fireball arise from the equilibrium between the fireball internal thermal pressure and the external compression pressure.

This condition takes the form:[13]

$$P_{\mathrm{th}}(T, \lambda_i, \gamma_i) = P_{\mathrm{dyn}} + P_{\mathrm{vac}}. \tag{26}$$

The thermal pressure follows in usual way from the partition function

$$P_{\mathrm{th}} = T/V \ln Z, \tag{27}$$

where aside of the temperature T, we encounter the different (quark and gluon) fugacities λ_i and the chemical saturation factors γ_i for each particle. For the vacuum pressure we will use:

$$P_{\mathrm{vac}} \equiv \mathcal{B} \simeq 0.1 \ \mathrm{GeV/fm}^3. \tag{28}$$

The pressure due to kinetic motion follows from well-established principles, and can be directly inferred from the pressure tensor[34]

$$T^{ij}(x) = \int p^i u^j f(x, p) \mathrm{d}^3 p, \quad i, j = 1, 2, 3. \tag{29}$$

We take for the phase-space distribution of colliding projectile and target nuclei

$$f_{\mathrm{P,T}}(x, p) = \rho_{\mathrm{P,T}}(x) \delta^3(\vec{p} \pm \vec{p}_{\mathrm{CM}}), \tag{30}$$

and hence in Eq. (29) $u^j = \pm \ p^j_{\mathrm{CM}}/E_{\mathrm{CM}}$. We assume that the nuclear density is uniform within the nuclear size, $\rho_0 = 0.16 \ /\mathrm{fm}^3$.

23

To obtain the pressure exerted by the flow of colliding matter, we consider the pressure component T^{jj}, with j being the direction of $\vec{v}_{\mathrm{CM}}$. This gives

$$P_{\mathrm{dyn}} = \eta_{\mathrm{p}} \rho_0 \frac{p_{\mathrm{CM}}^2}{E_{\mathrm{CM}}} \,. \tag{31}$$

Here it is understood that the energy E_{CM} and the momentum p_{CM} are given in the nucleon–nucleon CM frame and η_{p} is the momentum stopping fraction — only this fraction $0 \leq \eta_{\mathrm{p}} \leq 1$ of the incident CM momentum can be used by a particle incident on the central fireball (the balance remains in the unstopped longitudinal motion) in order to exert dynamical pressure. For a target transparent to the incoming flow, there would obviously be no pressure exerted. The simple expression Eq. (31) is illustrated in Fig. 10 as function of the stopping fraction. At current energies with stopping being above 50% we explore the conditions above 0.7 GeV/fm^3.

We now can determine the initial conditions reached in heavy ion collisions, since the two constraints, energy per baryon and pressure allow to fix the values of λ_{q} and T, provided that we make a hypothesis about the degree of chemical equilibration of the state considered. We are here primarily interested in determining the properties of the (near) chemical equilibrium state of the QGP-fireball, and its properties prior to its disintegration. As discussed in section 2 we assume that at about 1.5 fm/c in the CM frame the u, d quarks and gluons have reached their chemical equilibrium, i.e. $\gamma_{\mathrm{q}} \to 1$, $\gamma_{\mathrm{g}} \to 1$. But the strange flavor is still far from equilibrium and we choose $\gamma_{\mathrm{s}} \simeq 0.15$ appropriate for strange quark relaxation time being 7 times longer than the light quark one.[38] Because the QGP phase is strangeness neutral we have $\lambda_{\mathrm{s}} = 1$. Note here that the finite baryon density and baryon number conservation in the fireball force onto the system a rather large quark density, which is there from the beginning and needs not be produced; gluons are more easily produced than quark pairs and thus presumably their number catches up with the quark number by the time the collision has terminated — in baryon-free central region environments expected at much higher RHIC/LHC energies, the approach to chemical equilibrium can be different. The remaining statistical parameters T_{ch} and λ_{q} are now fixed by the EoS and are shown with other interesting properties of the fireball (number of gluons per baryon, number of light quarks and antiquarks per baryon, number of antistrange quarks per baryon, the pressure in the fireball, baryon density and the entropy per baryon) in the top segment of the table 1. The columns of table 1 correspond to the cases of specific experimental interest, in turn: Au–Au collisions at AGS, possible future Pb–Pb collisions at SPS with 40A GeV, S–Pb at 200A GeV, and for the Pb–Pb collisions at 158A GeV we considered two possible values of stopping, see Eq. (31): $\eta = 0.75$ and $\eta = 1$.

The difference between the two domains in table 1 is that in the bottom portion we have relaxed strange quarks to their equilibrium abundance (with exception of the S–W case for which we assume that strange quarks have reached 80% of phase space occupancy as suggested by the experimental results[4, 41]). During the formation of the strangeness flavor there is chemical cooling[42] and cooling due to (adiabatic) expansion of the fireball, in which $\lambda_{\mathrm{q}} = \mathrm{Const.}$, such that T decreases from T_{ch} to

24

Table 1: Properties and evolution of different collision systems.

Phase space occupancy	$<s-\bar{s}>=0$ $\lambda_s \equiv 1$	E/B [GeV]				
		2.6 $\eta=1$ Au–Au	4.3 $\eta=1$ Pb–Pb	8.8 $\eta=0.5$ S–Pb	8.6 $\eta=0.75$ Pb–Pb	8.6 $\eta=1$ Pb–Pb
$\gamma_q=1$	T_{ch} [GeV]	0.212	0.263	0.280	0.304	0.324
	λ_q	4.14	2.36	1.49	1.56	1.61
	n_g/B	0.56	1.08	2.50	2.24	2.08
$\gamma_g=1$	n_q/B	3.11	3.51	5.16	4.81	4.62
	$n_{\bar{q}}/B$	0.11	0.51	2.16	1.81	1.62
	$n_{\bar{s}}/B$	0.05	0.11	0.25	0.22	0.21
	P_{ch} [GeV/fm³]	0.46	0.76	0.79	1.12	1.46
$\gamma_s=0.15$	$\rho_{\rm B}$	3.35	3.31	1.80	2.45	3.19
	S/B	12.3	19.7	41.8	37.4	34.9
	γ_s	1	1	0.8	1	1
$\gamma_q=1$	T_0 [GeV]	0.184	0.215	0.233	0.239	0.255
	λ_q	4.14	2.36	1.49	1.56	1.61
$\gamma_g=1$	n_g/B	0.56	1.08	2.50	2.25	2.09
	n_q/B	3.11	3.51	5.12	4.81	4.60
	$n_{\bar{q}}/B$	0.11	0.51	2.12	1.81	1.62
$\gamma_s=0.8$	$n_{\bar{s}}/B$	0.34	0.68	1.27	1.43	1.33
or	P_0 [GeV/fm³]	0.30	0.41	0.47	0.54	0.71
$\gamma_s=1$	$\rho_{\rm B}$	2.17	1.80	1.05	1.19	1.56
	S/B	14.5	24.0	49.5	46.5	43.4

the full chemical equilibrium value T_0. We consider also this cooling in the simple model calculations devoted to the study of the strangeness production in section 6, see Fig. 24.

For the S–Pb/W collisions the temperature values shown in the bottom portion of the table are similar to the inverse slopes observed in particle spectra and shown in Fig. 9. Remarkably, the values of temperature T_0 found for the case of $E/B = 8.6$ GeV at $\eta = 0.5$ is just 233 MeV, which corresponds nearly exactly to the reported inverse slopes of the WA85 results,[23] and $\lambda_q = 1.49$ also agrees exactly with the results of our analysis,[4] also shown in Fig. 9. Even though there are a number of tacit and explicit parameters (in particular $\eta = 0.5, \alpha_s = 0.6$) we think that this result supports strongly the validity of our model involving the QGP fireball.

It is of interest for many applications to determine the initial fireball conditions systematically as function of the specific energy. In Fig. 11 we show as function of the specific energy content E/B, in top portion the behavior of temperature $T_{\rm ch}$ at which
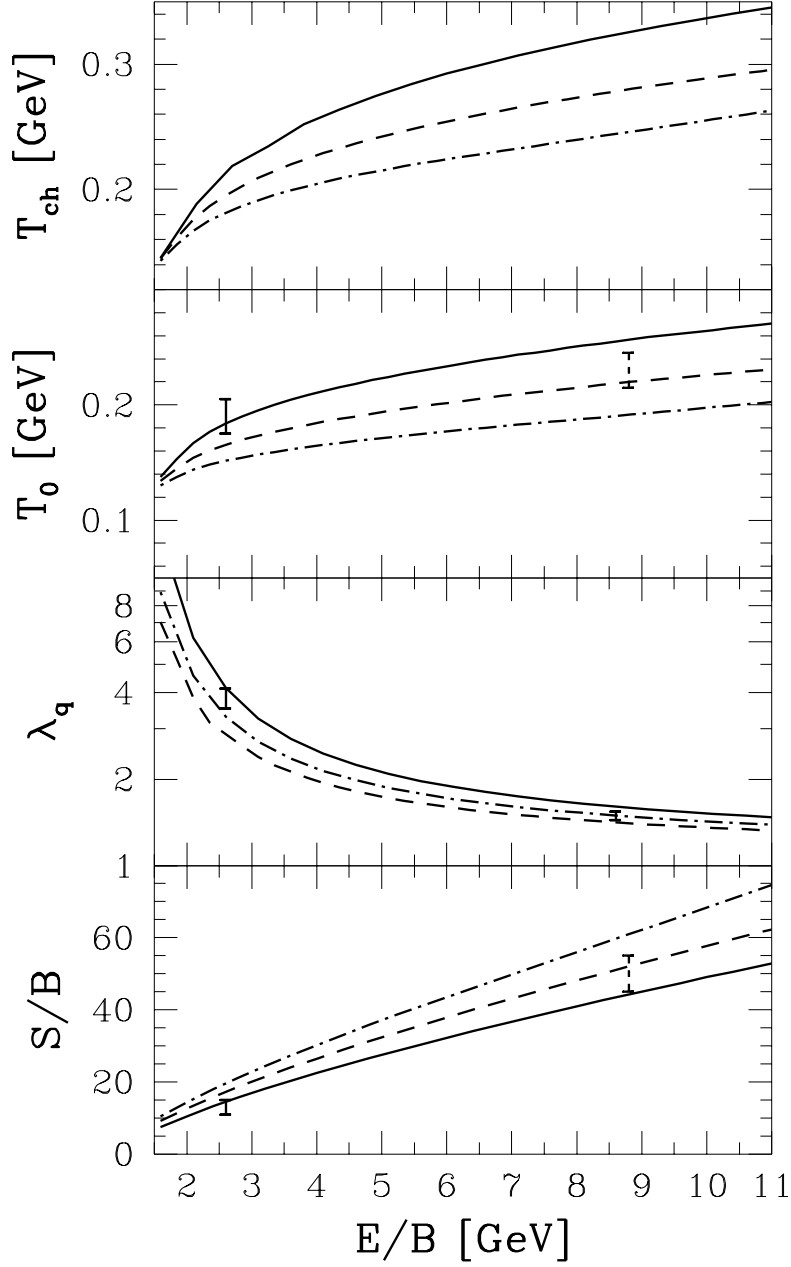
Figure 11: Initial fireball temperature T_{ch}, T_0, light quark fugacity λ_{q} and entropy per baryon S/B at the time of maximum chemical equilibration, as function of the QGP-fireball energy content E/B; stopping $\eta = 1$ (solid line), $1/2$ (dot-dashed line) and $1/4$ (dashed line). See text for comparison with analysis results.

light quarks and gluons have reached chemical equilibrium. Below it, we show values of T_0, determined by requiring that also strange quarks are in chemical equilibrium. In the next segment of the figure the fireball light quark fugacity λ_{q} and in the bottom section the entropy per baryon S/B at maximum chemical equilibration in the QGP

fireball. The experimental bars show, for high (8.8 GeV) energy, the result of the data analysis[4] discussed above, and those for low energy (2.6 GeV) are taken from the analysis of the AGS data.[18] The range of the possible values as function of η is indicated by showing the results for $\eta = 1$ (solid line), $1/2$ (dot-dashed line) and $1/4$ (dashed line). These results are in many respects fulfilling our expectations. We note the drop in temperature with decreasing energy and stopping; for a given specific energy the value of λ_q is relatively insensitive to the stopping power and there is a (rapid) rise of specific entropy with E/B.

5 Thermal Strangeness and Charm Production

The production of heavy flavor is a considerably slower process compared to the multitude of different reactions possible in a quark-gluon gas, which are leading to redistribution of energy between the available particles and to thermal equilibrium. Thus even if we assume, without microscopic understanding, that thermal equilibration is rapid, we should not expect the chemical (i.e. particle abundance) equilibrium to be present, especially so for heavy flavor. A well studied example of this situation is strangeness production.

We will evaluate in the following the dominant particle fusion contributions to the relaxation constant τ_s of strangeness. It has been computed using standard QCD methods[35] 15 years ago. However, doubts were raised if the perturbative methods applied lead to reliable results. Nonperturbative effects were more recently introduced[36] in terms of thermal temperature dependent particle masses. After the new production rates, including the now possible thermal gluon decay, were added up, the total strangeness production rate was found little changed. This finding was challenged,[37] but a more recent reevaluation of this work[38] confirmed that the rates obtained with perturbative glue-fusion processes are describing precisely the strangeness production rates in QGP, with $\tau_s \simeq 1.5$ fm/c for the here relevant $T > 250$ MeV temperature range, see Fig. 21 below. A full discussion of the current situation is given in a recent review[39] and we refer the interested reader for further details to this work. Here we note that what is probably happening is that the introduction of thermal masses amounts in essence to the replacement (in first order) of the gluon fusion processes by thermal gluon decay. Thus pending a full nonperturbative study of strangeness production in QGP medium, we will proceed here to describe strangeness production in terms of perturbative gluon and light quark fusion mechanisms displayed in Fig. 12.

We first consider these (angle averaged) flavor production cross sections. The evaluation of the lowest order diagrams shown in Fig. 12 yields[43]

$$\bar{\sigma}_{gg \to s\bar{s}}(s) = \frac{2\pi\alpha_s^2}{3s} \left[\left(1 + \frac{4m_s^2}{s} + \frac{m_s^4}{s^2} \right) \tanh^{-1} W(s) - \left(\frac{7}{8} + \frac{31m_s^2}{8s} \right) W(s) \right], \quad (32)$$

$$\bar{\sigma}_{q\bar{q} \to s\bar{s}}(s) = \frac{8\pi\alpha_s^2}{27s} \left(1 + \frac{2m_s^2}{s} \right) W(s), \quad (33)$$

where $W(s) = \sqrt{1 - 4m_s^2/s}$. We see in Fig. 13 that the magnitude of both cross sec-
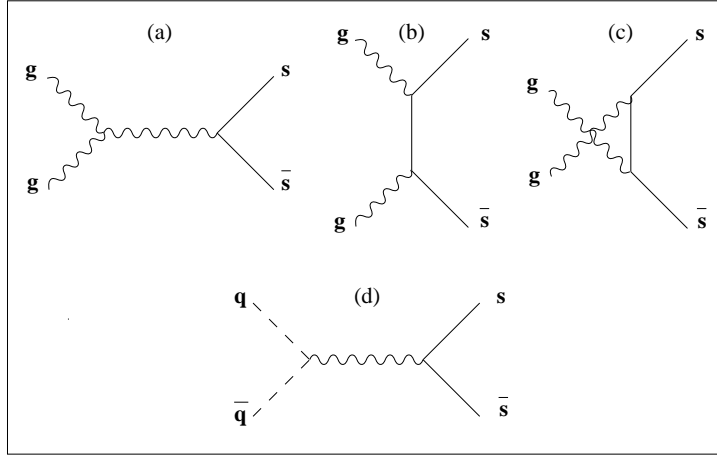
Figure 12: Lowest-order Feynman diagrams for production of $s\bar{s}$ (and similarly $c\bar{c}$) by gluon fusion and quark pair fusion.
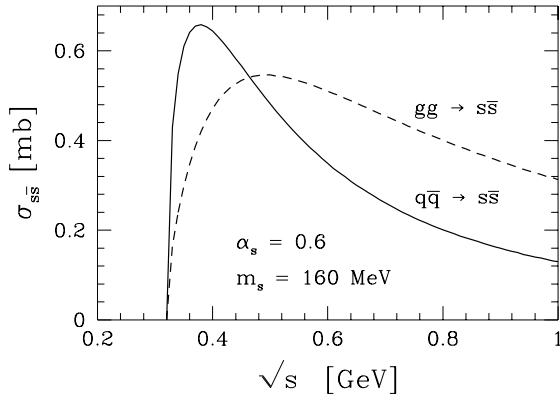
Figure 13: Strangeness production cross sections for $\alpha_s = 0.6$, $m_s = 160$ MeV.
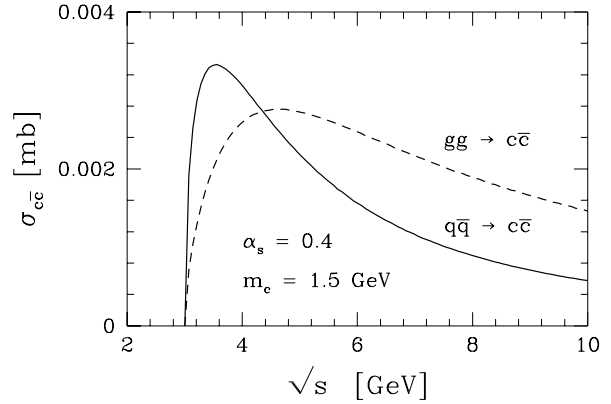
Figure 14: Charm production cross sections for $\alpha_s = 0.4$, $m_c = 1500$ MeV.

tions is similar. In Fig. 14 we show the gluon and quark-pair fusion charm production cross sections, computed for $m_c = 1500$ MeV and with reduced $\alpha_s = 0.4$, appropriate for the energy scale of charm production. Noteworthy is the smallness of this cross section, due to the relatively large value of $\sqrt{s}$ required, given that $\sigma \propto 1/s$. However, we will show that one cannot neglect the thermal charm production in LHC or even RHIC environments, where the charm production can lead in the end to notable phase space saturation at freeze-out.

With the production cross sections known, the net change in the strange quark abundance (and similarly charm, though here the annihilation rate is negligible) is given by the difference between the production and annihilation rates. Thus the evolution of flavor abundance in the QGP can be quite simply described by the population equation:

$$\frac{d\rho_s(t)}{dt} = \frac{d^4N(gg, q\bar{q} \to s\bar{s})}{dx^3\,dt} - \frac{d^4N(s\bar{s} \to gg, q\bar{q})}{dx^3\,dt} \ . \tag{34}$$

28

This can be expressed in terms of the thermally averaged cross sections $\langle \sigma v_{\rm rel} \rangle_T$ and particle densities ρ:

$$\frac{d\rho_{\rm s}(t)}{dt} = \rho_g^2(t)\,\langle \sigma v \rangle_T^{gg \to s\bar{s}} \; + \; \rho_q(t)\rho_{\bar{q}}(t)\langle \sigma v \rangle_T^{q\bar{q} \to s\bar{s}} - \rho_{\rm s}(t)\,\rho_{\bar{\rm s}}(t)\,\langle \sigma v \rangle_T^{s\bar{s} \to gg, q\bar{q}} \,. \qquad (35)$$

In chemical equilibrium, the strange quark density is a constant in time. Setting the left hand side of Eq.(35) equal to 0, we find the detailed balance relation for $t \to \infty$:

$$(\rho_g^\infty)^2 \, \langle \sigma v \rangle_T^{gg \to s\bar{s}} + \rho_q^\infty \rho_{\bar{q}}^\infty \langle \sigma v \rangle_T^{q\bar{q} \to s\bar{s}} = \rho_{\rm s}^\infty \, \rho_{\bar{\rm s}}^\infty \, \langle \sigma v \rangle_T^{s\bar{s} \to gg, q\bar{q}} \,. \qquad (36)$$

Eq.(36) relates the thermally averaged strangeness annihilation rate to the production rate. We substitute it into Eq.(35). Furthermore, since the kinetic and chemical equilibration of light quarks and gluons occurs on a considerably shorter time scale than the production of strangeness, we can assume that the gluon and light quark density is continually replenished through other channels so that

$$\rho_g(t) \to \rho_g^\infty; \quad \rho_q(t) \to \rho_q^\infty; \quad \rho_{\bar{q}}(t) \to \rho_{\bar{q}}^\infty \,,$$

and we obtain inserting this also into Eq.(35)

$$\frac{d\rho_{\rm s}(t)}{dt} \equiv \frac{dN_{\rm s}(t)}{dV\,dt} = (A_{gg} + A_{q\bar{q}}) \left[1 - \left(\frac{\rho_{\rm s}(t)}{\rho_{\rm s}^\infty} \right)^2 \right] \,, \qquad (37)$$

where we also have made use of the fact that $\rho_{\rm s}\rho_{\bar{\rm s}} = \rho_{\rm s}^2$ in QGP, and A is as defined by

$$A_{\rm AB} = \langle \sigma_{\rm AB}^s v_{\rm AB} \rangle_T \rho_{\rm A}^\infty \rho_{\rm B}^\infty \,. \qquad (38)$$

We can easily solve Eq.(37) analytically, when it is possible to assume that the (invariant) production rate $A = A_{q\bar{q}} + A_{gg}$ per unit volume and time is a constant in time:

$$\gamma_{\rm s}(t) \equiv \frac{\rho_{\rm s}(t)}{\rho_{\rm s}^\infty} \;=\; \tanh(t/2\tau_{\rm s}) \quad \text{for } A = \text{Const.} \qquad (39)$$

$$\simeq \; (1 - 2e^{-t/\tau_{\rm s}}) \quad \text{for } t > \tau_{\rm s} \,.$$

We see that the asymptotic limit is approached from below exponentially. $\tau_{\rm s}$ is referred to as the relaxation time constant, here for strangeness (and similarly charm) production in QGP and is given by

$$\tau_{\rm s} \equiv \frac{1}{2} \frac{\rho_{\rm s}^\infty}{(A_{gg} + A_{qq} + \ldots)} \,, \qquad (40)$$

where the dots indicate that other mechanisms may contribute to the heavy flavor production, further reducing the relaxation time. We can use series expansion to describe $\rho_{\rm s}^\infty$, the equilibrium abundance of heavy quarks and antiquarks in the QGP:

29
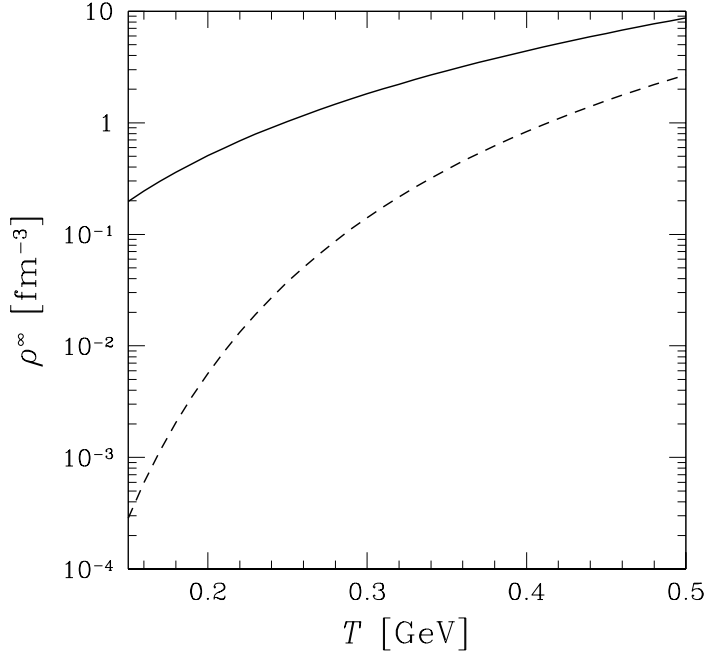
Figure 15: The statistical equilibrium density of strange or antistrange quarks with $m_s = 160$ MeV (solid line) and charmed or anticharmed quarks with $m_c = 1500$ MeV (dashed line) as function of temperature T.

since there is no strange chemical potential even at zero momentum their degeneracy is reduced by the factor $\exp(m_s/T)$, the expansion is everywhere convergent and we find

$$N_s^\infty = \frac{3}{\pi^2} V T^3 \, x^2 k_2(x) \,, \quad x = \frac{m_s}{T} \,, \tag{41}$$

where

$$k_2(x) \equiv \sum_{l=1}^{\infty} \frac{(-)^{l+1}}{l} K_2(lx) \,. \tag{42}$$

The first term in the expansion (42) leads to the Boltzmann approximation. The equilibrium density of strange ($m_s = 160$ MeV) and charmed ($m_c = 1500$ MeV) quarks is shown in Fig. 15.

We now determine the strangeness production rate:

$$A_s \equiv A_{gg} + A_{u\bar{u}} + A_{d\bar{d}} = \sum_{AB} \langle \sigma v_{AB} \rangle_T \rho_A^\infty \rho_B^\infty = \frac{dN(gg, q\bar{q} \to s\bar{s})}{d^3x \, dt} \,. \tag{43}$$

Thus the general expression for A_s is

$$
\begin{aligned}
A_s = & \int_{4m_s^2}^{\infty} ds \, 2s \delta(s - (p_A + p_B)^2) \int \frac{d^3 p_A}{(2\pi)^3 2E_A} \int \frac{d^3 p_B}{(2\pi)^3 2E_B} \\
& \times \left[\frac{1}{2} g_g^2 f_g(p_A) f_g(p_B) \overline{\sigma_{gg}}(s) + n_f g_q^2 f_q(p_A) f_{\bar{q}}(p_B) \overline{\sigma_{q\bar{q}}}(s) \right] \,,
\end{aligned}
\tag{44}
$$

30

where in principle the particle distributions f_i could be different from the thermal Bose/Fermi functions we will use here. The bar over the cross sections indicates that we use angle-averaged expressions. In order to obtain the above form, we have introduced a dummy integration over s and have employed for the relative velocity between two particles

$$
\begin{aligned}
v_{\mathrm{AB}} 2E_{\mathrm{A}} 2E_{\mathrm{B}} &\equiv & 2 \quad \lambda^{1/2}(s) \\
&=& 2 \quad \sqrt{s - (m_{\mathrm{A}} + m_{\mathrm{B}})^2} \sqrt{s - (m_{\mathrm{A}} - m_{\mathrm{B}})^2} \to 2s\,,
\end{aligned}
\tag{45}
$$

where the last limit holds for (nearly) massless particles.

We are interested to understand at which values of $\sqrt{s}$ the actual production processes occur, in order to establish the value of α_{s} we should employ. We rewrite the thermal production rate Eq.(44) as an integral over the differential rate dA/ds:

$$
A_i \equiv \int_{4m_{\mathrm{s}}^2}^{\infty} ds\, \frac{dA_i}{ds} \equiv \int_{4m^2}^{\infty} ds\, \overline{\sigma_i}(s)\, P_i(s)\,, \qquad i = g, q\,.
\tag{46}
$$

Here $P_g(s)ds$ is the number of gluon collisions within the interval of invariant mass $(s, s + ds)$ per unit time per unit volume, with a similar interpretation applying to $P_q(s)$. From Eq.(44) we find

$$
P_g(s) = \frac{1}{2} g_{\mathrm{g}}^2 \int \frac{d^3 p_{\mathrm{A}} f_g(p_{\mathrm{A}})}{(2\pi)^3 2E_{\mathrm{A}}} \frac{d^3 p_{\mathrm{B}} f_g(p_{\mathrm{B}})}{(2\pi)^3 2E_{\mathrm{B}}} 2s\delta(s - (p_{\mathrm{A}} + p_{\mathrm{B}})^2)\,,
\tag{47}
$$

$$
P_q(s) = n_{\mathrm{f}} g_q^2 \int \frac{d^3 p_{\mathrm{A}} f_q(p_{\mathrm{A}})}{(2\pi)^3 2E_{\mathrm{A}}} \frac{d^3 p_{\mathrm{B}} f_{\bar{q}}(p_{\mathrm{B}})}{(2\pi)^3 2E_{\mathrm{B}}} 2s\delta(s - (p_{\mathrm{A}} + p_{\mathrm{B}})^2)\,{}'
\tag{48}
$$

where P_q includes both u, d collisions in the factor n_{f} in an incoherent way, and hence $g_q = 2 \cdot 3$. For gluons we have $g_{\mathrm{g}} = 2 \cdot 8$. Assuming that the particle distributions depend only on the magnitude of the momentum, and using

$$
\delta(s - (p_A + p_B)^2) = \frac{1}{2 p_A p_B} \delta\left(\cos\theta - 1 + \frac{s}{2 p_A p_B}\right)\,,
\tag{49}
$$

we can carry out the two angular integrals to obtain:

$$
P_g = \frac{4}{\pi^4} s \int_0^{\infty} dp_A \int_0^{\infty} dp_B\, \Theta(4 p_A p_B - s) f_g(p_A) f_g(p_B)\,,
\tag{50}
$$

$$
P_q = \frac{9}{4\pi^4} s \int_0^{\infty} dp_A \int_0^{\infty} dp_B\, \Theta(4 p_A p_B - s) f_q(p_B) f_{\bar{q}}(p_B)\,.
\tag{51}
$$

The step function Θ arises because of the limits on the value of $\cos\theta$ in Eq.(49). To proceed, we assume thermal Bose and Fermi distribution for the particle distributions in the fireball rest frame. Possible $\vec{x}$-dependence is implicitly contained in T and μ_q:

$$
f_g(p) = \frac{1}{e^{p/T} - 1}\,,
\tag{52}
$$

$$
f_q(p) = \frac{1}{e^{(p-\mu_q)/T} + 1}\,,
\tag{53}
$$

$$
f_{\bar{q}}(p) = \frac{1}{e^{(p+\mu_q)/T} + 1}\,.
\tag{54}
$$

The integrals in Eqs.(50,51) can be carried out analytically, although only for $\mu_q = 0$ in the latter case. In this limit we have:

$$
\int_0^\infty dp_A dp_B \frac{\theta(4p_A p_B - s)}{(e^{p_A/T} \mp 1)(e^{p_B/T} \mp 1)} = \sum_{n=1}^\infty (\pm)^n \int_0^\infty \frac{dp_A}{(e^{p_b/T} \mp 1)} \int_{s/4p_B}^\infty dp_A \, e^{-np_A/T} ,
$$

$$
= \sum_{n,l=1}^\infty (\pm)^{n+l} \frac{T}{n} \int_0^\infty dp_B \, e^{-l\frac{p_B}{T}} e^{-n\frac{s}{4p_B T}} . \quad (55)
$$

This integral type is well known[44]

$$
\int_0^\infty dx \, e^{-\beta/4x} e^{-\gamma x} = \sqrt{\beta/\gamma} \, \mathrm{K}_1(\sqrt{\beta\gamma}) , \quad (56)
$$

and we obtain for the gluon case:

$$
P_g = \frac{4T s^{3/2}}{\pi^4} \sum_{l,n=1}^\infty \frac{1}{\sqrt{nl}} \, \mathrm{K}_1\left(\frac{\sqrt{nl\,s}}{T}\right) . \quad (57)
$$

Similar expression follows for quark processes when the chemical potentials vanish:

$$
P_q|_{\mu_q=0} = \frac{9T s^{3/2}}{4\pi^4} \sum_{l,n=1}^\infty \frac{(-)^{n+l}}{\sqrt{ln}} \, \mathrm{K}_1(\frac{\sqrt{nl\,s}}{T}) . \quad (58)
$$

The case with $\mu_q > 0$ is of greater physical interest in the present context of baryon-rich fireballs. In this case only the antiquark distribution (54) can be expanded in terms of a geometric series for all values of the quark momentum. Keeping the quark Fermi distribution, we obtain an expression containing one (numerical) integration

$$
P_q = \frac{9T}{4\pi^4} s \sum_{l=1}^\infty \frac{(-)^{l+1}}{l\lambda_q^l} \int_0^\infty dp_A \frac{e^{-l\frac{s}{4Tp_A}}}{\lambda_q^{-1} e^{p_A/T} + 1} , \quad (59)
$$

where $\lambda_q = e^{\mu_q/T}$ is the quark number fugacity. The remaining integral over dp_A has to be solved numerically. In Fig. 16 we show the collision distribution functions Eqs.(57,59) describing the probability that a pair of gluons (thick lines) or a light quark q–$\bar{q}$-pair (thin lines) collides at a given $\sqrt{s}$, for $T = 260$ (dotted) and 320 MeV (dashed), which we expect to be appropriate limits on initial fireball temperatures for the S–W and Pb–Pb collisions. For quarks we have taken $\lambda_q = 1.5$, which properly accounts for the baryon abundance in the fireball, see table 1. We also show $T = 500$ MeV (solid lines), with $\lambda_q = 1$, which choice, as we hope, is exploring the future conditions at RHIC/LHC. We note that since the mean energy per particle is approximately $3T$ in the relativistic gas, rather high $\sqrt{s}$ are reached, allowing in principle the thermal formation of charmed quark pairs.

The thermal differential production rates dA_i/ds for the flavor $i = s, c$, Eq.(46) are shown in Fig. 17 for strangeness and in Fig. 18 for charm. We note that for the

32
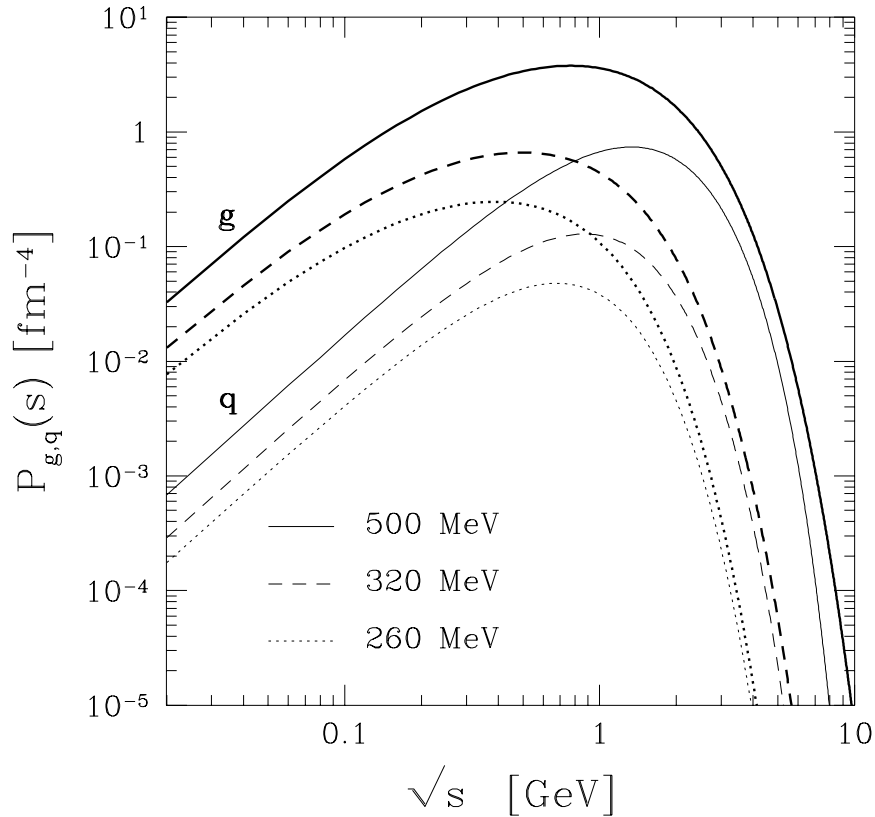
Figure 16: The collision distribution functions for gluons (thick lines) and quarks (thin lines) as function $\sqrt{s}$. Computed for temperature $T = 260$ MeV (dotted lines) and $T = 320$ MeV (dashed lines). For quarks $\lambda_q = 1.5$ was used in these two cases. The solid lines show the case of $T = 500$ MeV and $\lambda_q = 1$.

gluon fusion to strangeness processes the peak of the production occurs at $\sqrt{s} \simeq$ 0.5 GeV, and it is slightly more peaked and higher in energy than seen for quark pair processes. Thermal charm production peaks at $\sqrt{s} \simeq 3.5$ GeV, and we have allowed for this higher value of $\sqrt{s}$ by reducing the strength of the perturbative coupling constant. The dominance of the gluon channel in flavor production arises primarily from the greater statistical probability to collide two gluons in plasma at a given $\sqrt{s}$, as compared to the probability of $q + \bar{q}$ collisions, see Fig. 16 as well as from contributions at $\sqrt{s}$ away from production threshold.

The differential production rate can be easily integrated, and we show the results in Figs. 19 and 20. These results depend, of course, on the choice of the value of the strange and charmed quark mass, assumed here to be 160 MeV and 1500 MeV respectively. The result for charm production rate changes by 6–7 orders of magnitude as the temperature varies between 200 and 700 MeV. This sensitivity on the initial temperature, while understandable due to the fact that $m/T > 1$, also implies that since the charm production rate is not very small, we may have found an interesting probe of the primordial high temperature phase. This was also noted in a case study

33
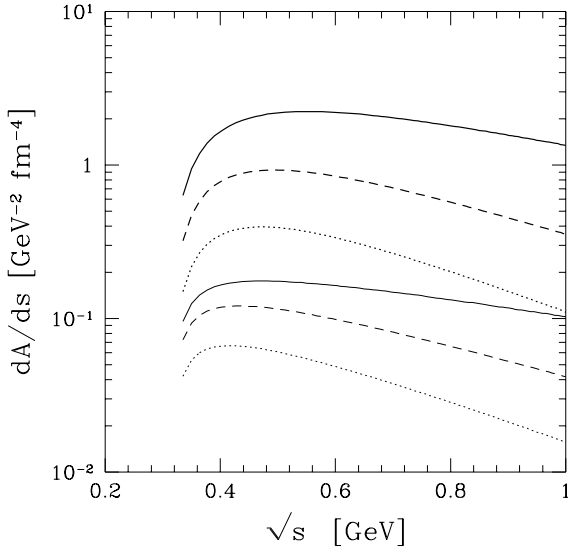
Figure 17: Differential thermal strangeness production rate $dA_s/ds = P(s)\sigma(s)$, with $T = 260$ MeV (dotted) and 320 MeV (dashed) and $m_\mathrm{s} = 160$ MeV, for gluons (thick) and $q\bar{q}$ pairs (thin), with $\lambda_q = 1.5$, $\alpha_\mathrm{s} = 0.6$; and for $T = 500$ MeV with $\lambda_q = 1$ and $\alpha_\mathrm{s} = 0.4$ (solid line).
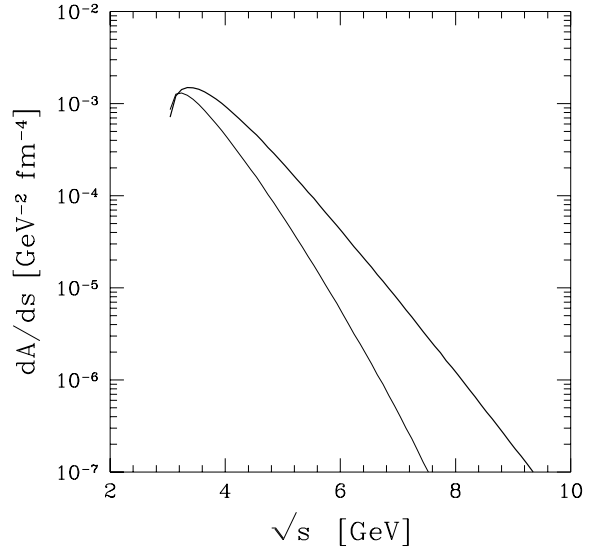
Figure 18: Differential thermal charm production rate $dA_\mathrm{c}/ds = P(s)\sigma(s)$, with $T = 500$ MeV, with $\lambda_q = 1$ and $m_\mathrm{c} = 1\ 500$ MeV, for gluons (thick) and $q\bar{q}$ pairs (thin, includes three flavors), with $\alpha_\mathrm{s} = 0.4$.

performed Levai *et al.*[45] Note that the gluon dominance of the production rate is not as pronounced for charm as it is for strangeness because charm formation occurs near to the threshold, where the quark fusion cross section dominates. Only for $T \geq 400$ MeV we find that the glue fusion dominates the charm production.

The production rates shown in Figs. 19 and 20 when inserted into Eq.(40) provide the relaxation time constants τ_s, τ_c. In Figs. 21 and 22 we show strangeness and charm relaxation constant. The dominance of gluon fusion over quark fusion for strangeness production process can be now more easily appreciated, and we note that as function of temperature in the interesting interval the relaxation time drops by an order of magnitude. This in particular explains the phenomenon, that when the QGP fireball cools, the abundance of strangeness freezes out, i.e., strangeness once produced is not reannihilated significantly.

For charm there is the well studied possibility that the thermal production is overwhelmed by the direct production based on high energy parton interactions. Calculations show[46] that per LHC event there may be a few directly produced charm quark pairs. On the other hand, the production rate of magnitude 10^{-2} fm^{-4} which we have obtained for an initial state with chemically equilibrated gluons at $T \simeq 700$ MeV implies that we should expect up to 20 thermal charmed quark pairs per such event, centered at central rapidity. Consequently, we continue below to evaluate in detail the evolution of thermal charm yield, which may dominate the production rate and in particular lead to rather surprising features in final particle yields, should the
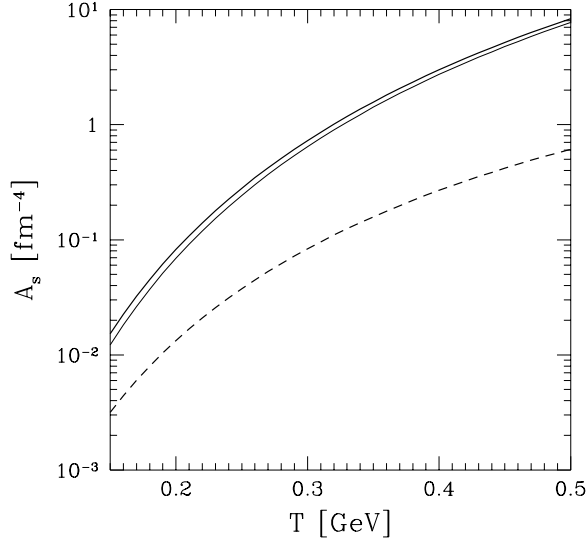
Figure 19: Thermal strangeness production rates A_s in QGP: total (thick solid line), gluons only (thin solid line), and light quarks only (dashed line), calculated for $\lambda_q = 1.5$, $m_s = 160$ MeV, $\alpha_s = 0.6$ as function of temperature.
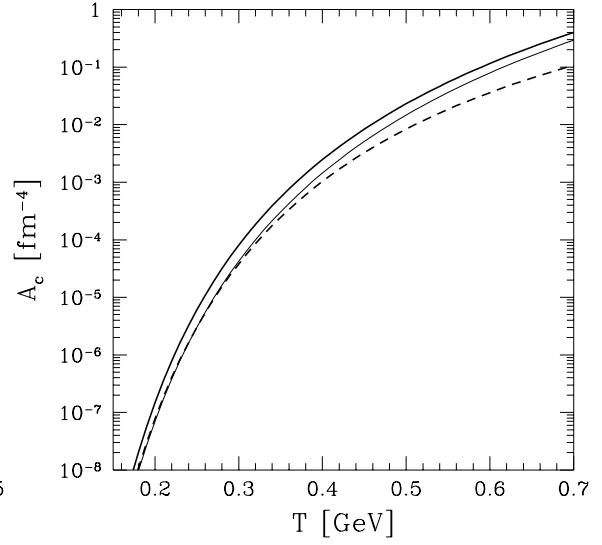
Figure 20: Thermal charm production rates A_c as function of temperature in QGP: total (thick solid line), gluons only (thin solid line), and light quarks only (dashed line), calculated for $\lambda_q = 1$, $m_c = 1500$ MeV, $\alpha_s = 0.4$.
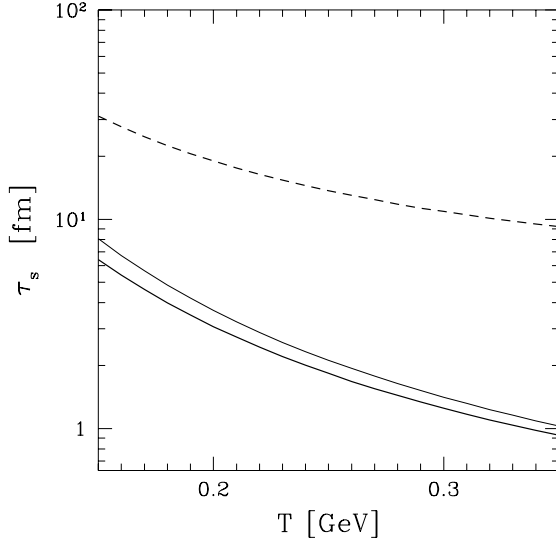
Figure 21: Thermal strangeness relaxation constants in QGP: same conventions and parameters as in Fig. 19.
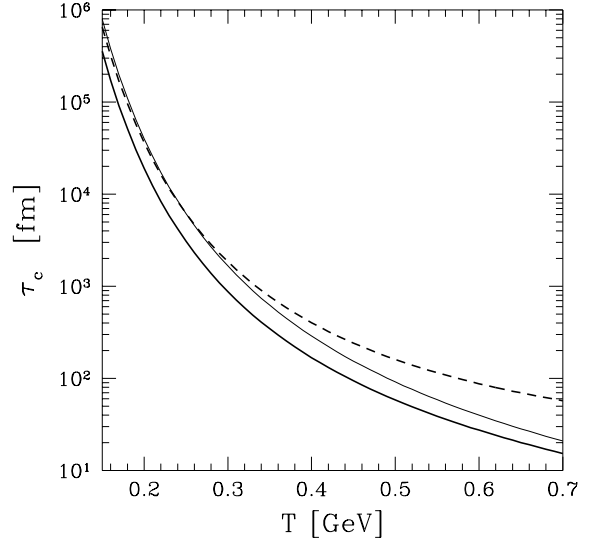
Figure 22: Thermal charm relaxation constant in QGP: same conventions and parameters as in Fig. 20.

initial plasma temperature be sufficiently large.

We wish to record here that the strangeness phase space saturation seen in SPS-relativistic heavy ion collision experiments cannot be a simple result of totally con-

35
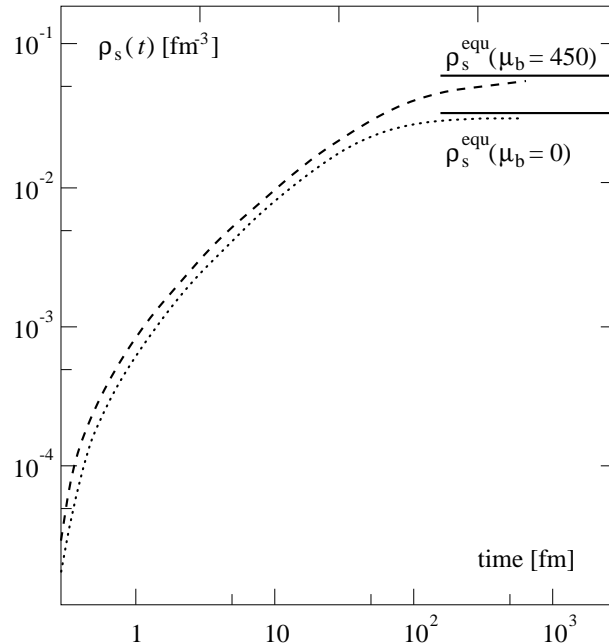
Figure 23: Thermal strangeness production as function of time in a confined hadron gas at $T = 160$ MeV. Results for two values of baryochemical potential ($\mu_B = 0$ and 450 MeV are shown. After Koch *et al.*[49]

ventional physics. In the dense state of highly excited confined HG fireball, there are many different strangeness production channels and a full discussion is beyond the scope of this presentation. The key results were described in detail elsewhere:[48,49] in a gas consisting of particle states with normal properties, strangeness saturation time scales are very much longer, as is shown in Fig. 23, where the approach to equilibrium abundance as function of time takes nearly 100 fm/c. Thus if this was the actual situation, then the strange particle abundance would be largely result of pre-thermal collisions, and thus could be easily described by folding of a geometric microscopic collision model with the experimental N–N results. There is considerable ongoing effort to simulate, using microscopic models, this initial phase of nuclear collisions, and while these efforts can produce appropriate yields of some particles, the overall reaction picture,[27] in particular considering the multi-strange baryons and antibaryons is so far not satisfactory, supporting at least the claim that strangeness enhancement requires some new physics phenomenon, if not QGP as we are arguing here. Models that include microscopic deconfinement, such as the dual parton model,[47] but which do not assume thermalization, require the introduction of parameters to fit the multi-strange particle yields at central rapidities.

6   Temporal Evolution of Heavy Quark Phase Space Occupancy

As we have discussed in section 3 it is rather straightforward to extract, from the strange antibaryon experimental particle yields,[4,5,14] the value of γ_s, since its hadro-

nisation value governs the particle ratios involving different strangeness content. Since $\tau_{\rm s}$ is just of the magnitude of the life span of the deconfined state, see Fig. 21, strangeness will be close to fully saturate the final state phase-space in the QGP fireball. However, this accidental similarity of the life span of the fireball and the relaxation time of strangeness implies that changes in the collision conditions should lead to measurable changes of $\gamma_{\rm s}$. This would be a highly desirable situation, allowing a test of the theoretical predictions. It can be expected that in the near future $\gamma_{\rm s}$ will be studied varying a number of parameters of the collision, such as the volume occupied by the fireball (varying size of the colliding nuclei and impact parameter), the trigger condition (e.g. the inelasticity), the energy of colliding nuclei when searching for the threshold energy of abundant strangeness formation. We thus develop in this section a more precise understanding of the observed value of $\gamma_{\rm s}$, as function of the collision parameters.

Similarly, as alluded to above in section 5, the thermal charm production is sensitive to the initial temperature, but clearly the production of charmed particles will not saturate the initially available phase space. However, it is interesting to see what values of $\gamma_{\rm c}$ would be found in the final state, since the equilibrium density of charm at hadronisation is very low. Also here we need to consider in some more detail the temporal evolution with the plasma expansion of the off-equilibrium parameter $\gamma_{\rm c}$.

Since the thermal equilibrium is by hypothesis established within a considerably shorter time scale than the (absolute) heavy flavor chemical equilibration, we can characterize the saturation of the phase space by an average over the momentum distribution, see also Eq. (39)

$$\gamma_{\rm s,c}(t) \equiv \frac{\int d^3p\, d^3x\, n_{\rm s,c}(\vec{p}, \vec{x}; t)}{\int d^3p\, d^3x\, n_{\rm s,c}^\infty(\vec{p}, \vec{x})} \ , \tag{60}$$

where $n_{\rm s,c}$ is the sum over all heavy flavor containing particle densities, and should multi-strange/charmed objects be present, this sum contains the associated weight. $n_{\rm s,c}^\infty$ is the same, but for the equilibrium particle densities. In QGP deconfined state, of course we have just the free quarks. When the $\vec{x}$ dependence is contained solely in the statistical parameters we have:

$$n_{\rm s}(\vec{p}, \vec{x}; t) \simeq \gamma_{\rm s}(t) n_{\rm s}^\infty(\vec{p}; T(\vec{x}, t), \mu_{\rm s}(\vec{x}, t)) \, . \tag{61}$$

A further refinement should be noted: when the quantum aspects of the particle distributions are incorporated and the maximum entropy state of an isolated physical system (closed system) is obtained, the relative chemical equilibrium coefficients γ_i enter as multiplicative coefficients in front of the Boltzmann factor within the quantum Bose/Fermi distribution, along with the fugacity factors:[42]

$$n_i^{\rm B,F} = \frac{1}{\gamma_i^{-1} \lambda_i e^{\beta \epsilon_i} \mp 1} \ \rightarrow \ \gamma_i \lambda_i^{-1} e^{-\beta \epsilon_i} \, . \tag{62}$$

The subtle difference between γ and λ is that while the latter is conjugated between particles and antiparticles, see Eq.(4), γ is the same for particles and antiparticles.

We begin with the general expression for strangeness production, Eq.(37). Taking the particle density everywhere in the fireball as constant, we have:

$$\frac{1}{V}\frac{dN_s(t)}{dt} = A\left[1 - \gamma_s^2\right] . \tag{63}$$

It is common practice to write $N = \rho V$ which when inserted on the left hand side of Eq.(63) leads to:

$$\frac{d\,\rho_s}{dt} + \rho_s\frac{1}{V}\frac{dV}{dt} = A\left[1 - \gamma_s^2\right] . \tag{64}$$

The second term on the left hand side is referred to as the volume dilution term.

In order to obtain a dilution equation for γ_s, let us instead proceed, using in Eq.(63) the definition of γ_s in the form:

$$N_s(t) = \gamma_s(t)N_s^\infty(T(t)) . \tag{65}$$

Note that when dividing Eq.(65) by $V(t)$ we recover our earlier definitions of γ_s, see Eqs.(39,61).

Inserting Eq.(65) into Eq.(63) we obtain:

$$2\tau_s\left(\frac{d\gamma_s}{dt} + \gamma_s\frac{d}{dt}\ln N^\infty\right) = 1 - \gamma_s^2 . \tag{66}$$

It is noteworthy that N^∞, the final total abundance of particles, as given in Eq.(41), changes only slowly in time when the volume and temperature temporal evolution is governed by the adiabatic evolution condition:

$$V \cdot T^3 = \text{Const.} . \tag{67}$$

Thus the logarithmic derivative in the dilution term in Eq.(66) is in many cases very small since:

$$\frac{d}{dt}\ln N^\infty = \frac{d}{dt}\ln\left(x^2k_2(x)\right) ; \quad x = \frac{m}{T(t)} . \tag{68}$$

What we see happening is that the volume dilution seen in Eq.(64) is nearly completely compensated by the dilution of the value of $\rho^\infty(T)$ in presence of adiabatic cooling.

In many cases it is sufficient to study an approximate solution of Eq.(66). For $m_s/T = x < 1$ we have $x^2k_2(x) \simeq \text{Const.}$, and hence we have the analytical solution

$$\gamma_s \simeq \tanh\left(\int_0^{t_{\text{freeze}}} \frac{dt}{2\tau_s(T(t))}\right) < 1 , \quad m_s/T < 1 , \tag{69}$$

where the semi-convergent approximation[35] for the dominant gluon fusion term has been used in the past[35]

$$\tau_s^g m_s = \alpha_s^{-2}\frac{9}{7}\sqrt{\frac{\pi}{2}}\frac{x^{5/2}}{e^{-x}(x + 99/56 + \ldots)} , \tag{70}$$

in order to argue that the value of $\gamma_{\rm s}$ in many cases of interest approaches unity.

But the approximate solution, Eq.(69) presumes that the final freeze-out occurs such that $m_{\rm s}/T < 1$, which condition is not fulfilled if the plasma hadronises at temperatures of the magnitude $T = 140$ MeV as seems to be the case today for the baryon rich plasma, see our discussion in section 8 and the results of lattice gauge simulations of QCD.[1] We will now show numerically that major deviations from the approximate solution arise and in particular $\gamma_{\rm s}$ can easily become much greater than unity, depending on the precise value of the freeze-out temperature. To see this note that a slight rearrangement of Eq.(66) leads to the form:

$$\frac{d\gamma_{\rm s}}{dt} = \left(\gamma_{\rm s} \frac{\dot{T} m_{\rm s}}{T^2} \frac{d}{dx} \ln x^2 k_2(x) + \frac{1}{2\tau_{\rm s}} \left[1 - \gamma_{\rm s}^2 \right] \right) , \tag{71}$$

which shows that even when $1 - \gamma_{\rm s}^2 < 1$ we still can have a positive derivative of $\gamma_{\rm s}$, since the first term on the right hand side of Eq.(71) is always positive, both $\dot{T}$ and $d/dx(k_2)$ being always negative. Note that $1/\tau$ becomes small when T drops below $m_{\rm s}$ and whence the dilution term dominates the evolution of $\gamma_{\rm s}$.

In order to perform a more complete, numerical study of the dependence of γ on the system parameters, we need to know how the temperature, which enters explicitly in Eq.(71) and implicitly through the relaxation constant $\tau_{\rm s}$, depends on time. In our earlier discussion in section 2 we have not modeled in full the cooling arising in a free flow of the fireball matter. It is a rather complicated matter to account simultaneously for both the chemical cooling, due to the strangeness production, and the flow cooling arising from volume expansion. Given the qualitative nature of our following study we shall concentrate here only on the flow cooling and ignore the impact of chemical cooling. We therefore denote all initial values by the index 'in' in order to distinguish our present simple and schematic model from our earlier discussion and more refined approaches. For the current series of SPS experiments we assume that the volume of the fireball expands adiabatically in all directions at maximal sound velocity $v_c = c/\sqrt{3}$. Thus we have assumed for the fireball radius

$$R = R_{\rm in} + \frac{1}{\sqrt{3}} (t - t_{\rm in}) , \tag{72}$$

and hence from the adiabatic expansion constraint Eq.(67) we obtain the time dependence:

$$T = \frac{T_{\rm in}}{1 + \frac{t - t_{\rm in}}{\sqrt{3} R_{\rm in}}} . \tag{73}$$

A sensible set of initial conditions for the SPS experiments, dictated by the global event structure and the hadronic freeze-out seen in HBT experiments[50] is:

$T_{\rm in} = 320$ MeV; $R_{\rm in} = 5$ fm; $t_{\rm in} = 1$ fm/c; $\lambda_{\rm q} = 1.6$; for Pb–Pb at 160A GeV,
$T_{\rm in} = 260$ MeV; $R_{\rm in} = 3$ fm; $t_{\rm in} = 1$ fm/c; $\lambda_{\rm q} = 1.5$; for S–Pb at 200A GeV.
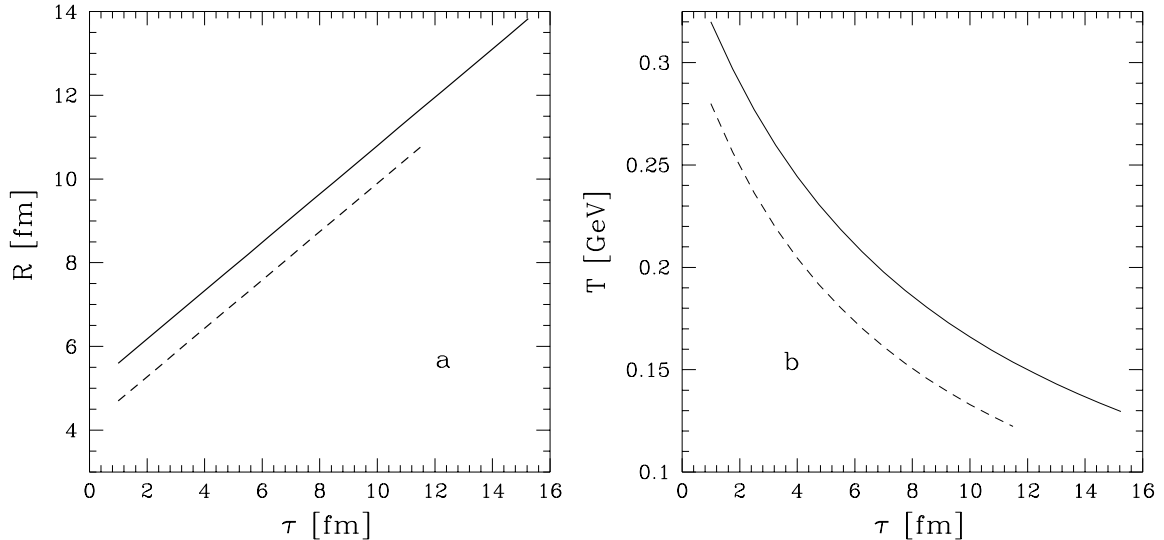
Figure 24: Assumed temporal evolution (see Eqs. (72,73) of **a**) the radius parameter $R(t)$ and **b**) temperature T of the thermal fireball formed in Pb–Pb collisions (solid lines) and S–W/Pb collisions (dashed lines).

Also, we take $\gamma_s(t = t_{\rm in}) = 0.15$ as the initial strangeness abundance after 1 fm/c. The chosen values of $\lambda_{\rm q}$ are of minimal importance, as they enter marginally into the quark-fusion rate, which is a minor contribution to the strangeness production rate. The important global parameters used are $\alpha_s = 0.6$ and $m_{\rm s} = 160$ MeV.

The here implied temporal variation of $R(t)$, $T(t)$ is presented in Fig. 24. We note that the temperature drops to the commonly accepted phase transition value[1] $T = 150$ MeV after 5 and 11 fm/c for S–W/Pb and Pb–Pb systems, respectively. At this point the size of the fireball has reached 7 and 11 fm, respectively.

The numerical integration of Eq.(71) is now possible, up to the point at which the plasma phase ceases to exist or/and the final state strange particles are emitted. According to our hypothesis, which leads to a successful interpretation of the experimental data, the abundances of rarely produced strange (anti)baryons is not further affected by subsequent evolution. We present γ_s for the case of S–W/Pb collisions (dashed lines) and Pb–Pb collisions (solid lines), in Fig. 25**a** as function of final time and in Fig. 25**b** as function of final temperature. We note that for 8 fm/c we obtain the observed value $\gamma_{\rm s} \simeq 0.75$ for the S–W/Pb collisions. However, this time is associated with a low final temperature of $T = 110$ MeV, as can be deduced from the result shown in Fig. 25**b**. Taking the final temperature value to be $T \simeq 140$ MeV, the value we found[5] for the S–W/Pb case, one arrives at $\gamma_{\rm s} \simeq 0.57$. This is slightly less than the experimental result $\gamma_{\rm s} \simeq 0.75$ which suggests that our ideal flow temporal evolution model may be leading to a too fast cooling or/and that the perturbative estimate of the strangeness production rate is a bit too low — to reach exact agreement between experiment and theory we would need a cumulative change in these two here relevant quantities (flow velocity and QGP-strangeness production rate) of magnitude 20%. There is clearly plenty of room for an improvement of this magnitude in both these

40
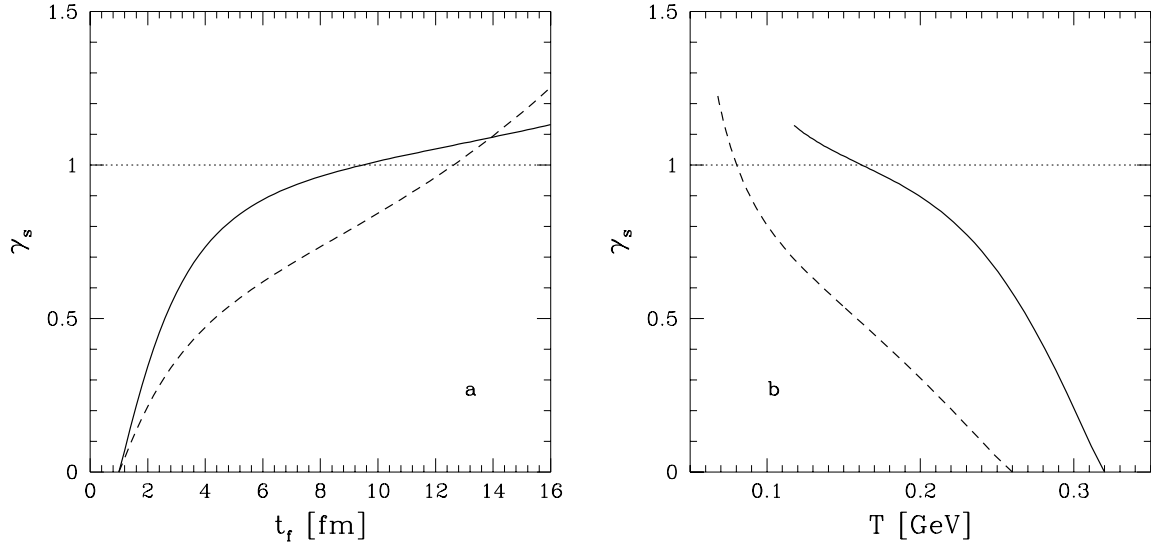
Figure 25: QGP-phase strangeness phase space occupancy γ_s **a** as function of time and **b** as function of temperature, for $\alpha_s = 0.6$ and $m_\mathrm{s} = 160$ MeV, for initial conditions pertinent to maximum SPS energies (200A GeV S beam and 158A GeV Pb beam). Solid lines: conditions relevant to central Pb–Pb interactions, dashed lines: conditions relevant to S–W/Pb interactions (see table 1).

quantities.

When considering the Pb–Pb collisions we are primarily interested to find if it is likely that we reach $\gamma_\mathrm{s} = 1$. For this to occur, our results, see Fig. 25, suggest that the final QGP fireball temperature should be lower than 160 MeV. Note that allowing for the above discussed likely further increase in production rate and/or reduction in flow, pushes this temperature limit to 210 MeV. We thus can be practically certain that in Pb–Pb collisions at 158A GeV one observes $\gamma_\mathrm{s} \geq 1$ with the associated interesting consequences for strange particle abundances (see section 8).

To study the dependence on the impact parameter on strangeness saturation, we vary the magnitude of the initial fireball size R_0. From geometric considerations one finds roughly the relation between the impact parameter b in Pb–Pb collisions, and R_in to be $R_\mathrm{in} \simeq (6 - b/2)$ fm > 0; for small impact parameters, $0 < b < 2$ fm, we assume here formation of a 'standard' fireball of 5 fm radius. A further assumption is needed regarding initial temperature of the fireball: we will not vary this parameter, leaving it for the Pb–Pb collisions at $T_\mathrm{in} = 320$ MeV for all fireball sizes. However, for larger impact parameters (small fireball sizes) the actual pressure stopping is reduced and thus the heating and compression of the fireball is less than we have implicitly assumed using a constant value for T_in for different initial fireball volumes. It is impossible for us to improve on this hypothesis here, since this requires the understanding of the hadronic matter stopping as function of the amount of hadronic matter involved. With this set of initial conditions we integrate the dynamical equation Eq. (71) for γ_s up to final temperature $T \simeq 140$ MeV (see discussion below in section 7) for the 200A GeV S–W/Pb collisions. We find that full strangeness phase space saturation occurs for fireballs with a radius $R_\mathrm{in} > 4$ fm, which includes impacts parameters b

41
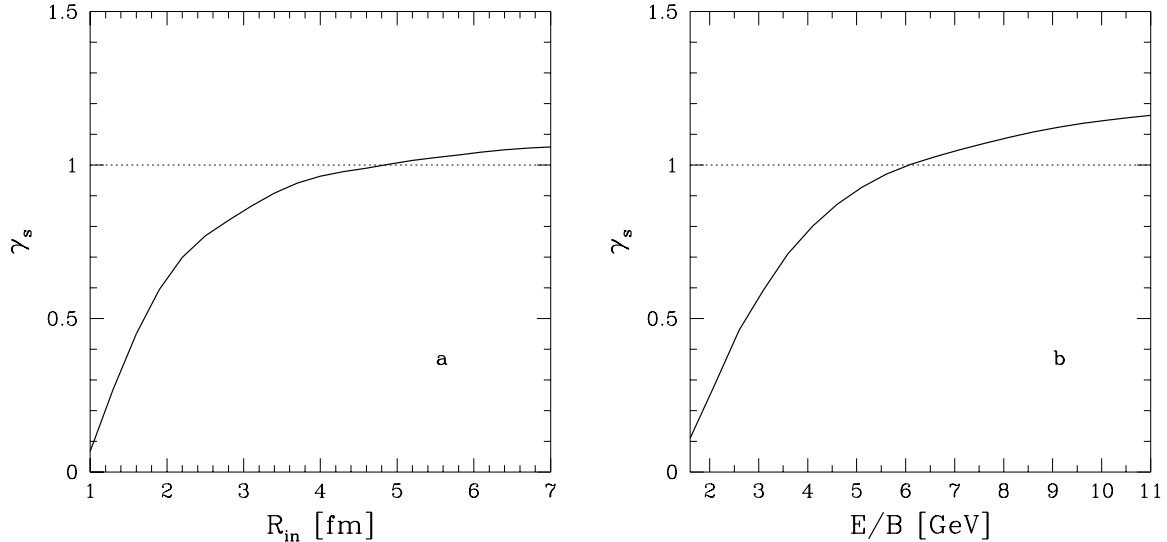
Figure 26: Strangeness phase space occupancy **a** as function of initial fireball size R_{in} assuming initial conditions of the zero impact parameter 158A GeV Pb–Pb collisions; **b** as function of the CM-specific ion collision energy content, assuming a $R_{in} = 5$ fm initial fireball size and freeze-out at 140 MeV.

up to about 3–4 fm. This result suggests that there is no need to trigger onto very central collisions in order to observe $\gamma_s \simeq 1$. Moreover, the relatively sudden onset of the phase space saturation seen in Fig. 26**a** as function of fireball size is very probably even more sudden, had we incorporated the changing stopping related to the change of volume.

It is also most interesting to study how γ_s depends on the Pb–Pb collision energy. We obtain this result by varying the initial fireball temperature T_{in} and relating this value to the specific energy content in the fireball by the results given in Fig. 11 — we take here the result we obtained for full stopping $\eta = 1$. Recall that baryon and energy stopping being equal, $E/B = 8.6$ GeV corresponds to 158A GeV Pb–Pb collisions. For each initial temperature T_{in} we assume that the initial value of γ_s is 0.15, and integrate the temporal evolution of γ_s, Eq. (71), till the final temperature which is taken for all collision energies to be at $T = 140$ MeV. As shown in Fig. 26**b** for the full SPS range $4.3 < E/B < 8.6$ GeV we find as expected fully saturated phase space, with $0.8 < \gamma_s < 1.1$. Between the AGS $E/B = 2.6$ GeV and CERN energies γ_s increases from 0.45 to 0.85. We recall that our study of the S–Pb collision system suggests somewhat more effective chemical equilibration, thus the small variation of γ_s with energy reported here may be even less pronounced. On the other hand this small variation impacts the final particle yields as we shall see in section 8, in that it makes relative yields of strange antibaryons such as $\overline{\Lambda}/\bar{p}$, $\overline{\Xi}/\overline{\Lambda}$ nearly independent of collision energy.

We can now briefly return to the discussion of the result of the NA35[29] collaboration shown in Fig. 5: despite the large error bar it is noticeable that there is a tendency for the $\overline{\Lambda}/\bar{p}$-ratio to increase as the collision system becomes smaller. This

42
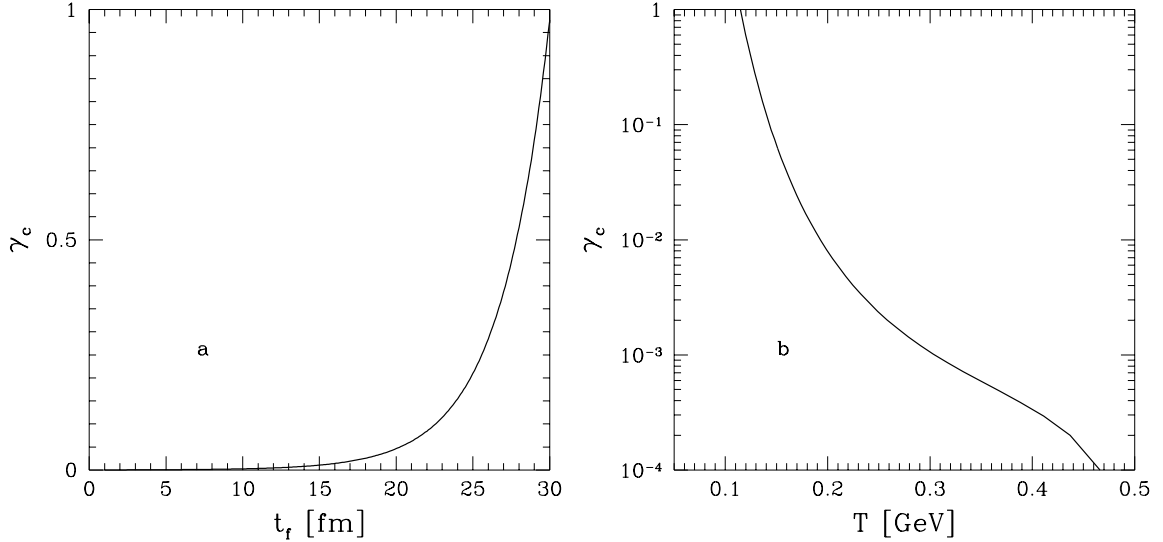
Figure 27: QGP phase charm phase space occupancy γ_c in central Pb–Pb interactions: **a** as function time and **b** as function of temperature, for $\alpha_s = 0.4$.

can be interpreted in terms of γ_s and one finds the normally perplexing result that while S–Au collisions lead to $\gamma_s \simeq 0.8 \pm 0.2$, the S–S collisions may require a greater value $\gamma_s \simeq 1.2 \pm 0.3$. In the earlier analysis[4] of S–S data (excluding $\bar{p}$) this tendency towards $\gamma_s \simeq 1$ was also found, while the S–W/Pb results always invariably lead to $\gamma_s \simeq 0.75$. While it is hard to imagine, it is not anymore impossible in light of the model calculations done above, that the combination of initial and disintegration conditions of these two systems reverses the naive expectations regarding the final observable values of γ_s.

We now explore the saturation of the charmed quark phase space in conditions sensible for the forthcoming RHIC and LHC environments. We consider the temporal evolution for the initial temperature 500 MeV. Due the to likely dominance of the expansion by the longitudinal flow we take for the adiabatic condition the relation $LT^3 = \text{Const}$. We take that L expands with light velocity. As can be seen in the results shown in Fig. 27 thermal production of charm is small, being very slow, but because the freeze-out temperature should here also be taken in the vicinity of 150 MeV, the phase space occupancy reaches a stunning value 6%. Still greater values result for higher initial temperatures and/or lower freeze-out temperatures. We note that the discussion of thermal charm production in this language makes only sense if the number of charmed quark pairs produced in the initial moments is considerably greater than unity. We thus present in Fig. 28 the pair yield as function of initial temperature (assuming small impact parameter collisions). We note that our calculations apply to initial temperatures above 500 MeV and that for $T_{\text{in}} = 700$ MeV we would be reaching a yield of twenty charm quark pairs.

43
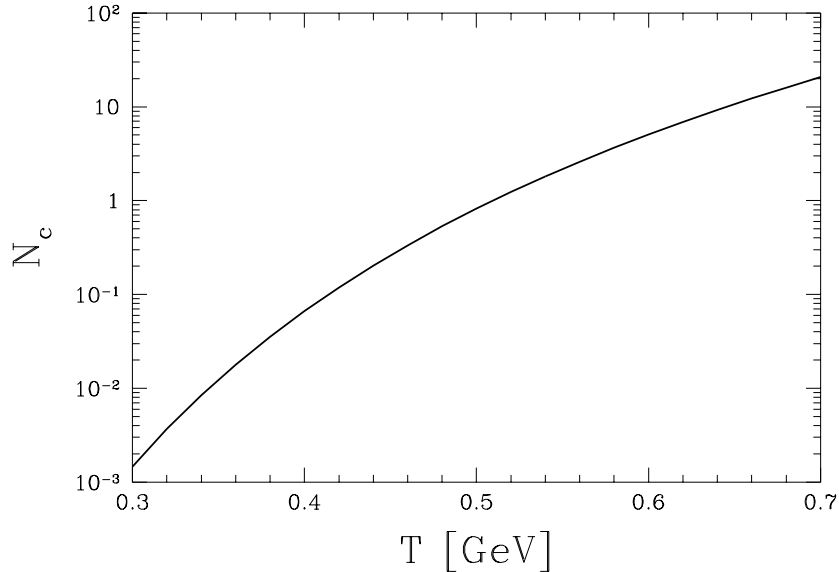
Figure 28: Total charm production yield in longitudinally expanding QGP as function of initial temperature.

7   Hadronisation Model

It is easy to imagine QGP-hadronisation mechanisms that would largely erase memory of the transient deconfined phase. We will not discuss such *re-equilibrating* hadronisation models[51] of strange particles which are not observed at least at SPS energies.[4] Instead, we shall focus our attention on the alternative that the particles emerge directly and without re-equilibration from the deconfined phase.

Our approach to hadronisation and particle production is schematic and does not involve development of a dynamical model.[17] Instead we introduce two parameters which describe how far are from the hadronic gas equilibrium the produced meson and baryon abundances — there is no reason whatsoever to expect that the rapid disintegration of the deconfined state will lead to particle abundances that are associated with full chemical equilibrium of any individual particle species in the final state. These hadron nonequilibrium constants C_i are in principle different for each particle species, but if we presume that the mechanisms that lead to particle production are similar for all mesons ($i = $ M), and all baryons ($i = $ B), we can group all particles into these two families, keeping just two unknown quantities. Note that also the *relative* abundances of mesons and baryons emerging from hadronising QGP are difficult to equilibrate, because processes which convert meson into baryon-antibaryon pairs are relatively slow. The magnitude of these abundance coefficients C_i is determined theoretically by the need to conserve or increase entropy, conserve baryon number and strangeness in the hadronisation process.

The abundance of particles emerging is, according to Eq. (2), determined by the

normalization constant

$$N_j = C_j V \prod_i n_i \,, \qquad n_i = g_i \gamma_i \lambda_i \,, \qquad j = \mathrm{M,\ B} \,, \tag{74}$$

where it is assumed that the final state particle of type j contains the quark valence components of type i and these are counted using their statistical degeneracy g_i, fugacity $\lambda_i = \exp(\mu_i/T)$ and the chemical equilibration factor γ_i. V is the emission source volume. Fragmentation of gluons contributes to the active quark abundance and has been considered previously.[15] Because it enhances the number of all quarks and the effect is weighted in a similar way for all flavors, and further, since in the ratio of particle abundances a partial cancelation of this effect occurs, this effect is apparently of lesser importance for the ratios of particles, but of essence to increase the yield of particles at small $m_\perp$. Once chemical non-equilibrium features are accounted for by three significant abundance factors $\gamma_s, C_{\mathrm{M,B}}$, the chemical potentials for particles and antiparticles are opposite to each other and the particle and antiparticle abundances are related, see Eq. (4). As indicated in Eq. (74), the fugacity of each final state hadronic species is the product of the valence quark fugacities.

We now consider strangeness conservation in the final state: the abundances of the final state strange particles can be gauged by considering the Laplace transform of the phase space distribution which leads to a partition function *like* expression $\mathcal{Z}_s$. The individual components comprise aside of the chemical factors λ_q and λ_s, the non-equilibrium coefficients γ_s, C_{B}^s and C_{M}^s. (we have added here the superscript 's' to the factors C since at present we look only at strange particles):

$$\ln \mathcal{Z}_s = \frac{VT^3}{2\pi^2} \Big\{ (\lambda_s \lambda_q^{-1} + \lambda_s^{-1} \lambda_q) \gamma_s C_{\mathrm{M}}^s F_K + (\lambda_s \lambda_q^2 + \lambda_s^{-1} \lambda_q^{-2}) \gamma_s C_{\mathrm{B}}^s F_Y$$
$$+ (\lambda_s^2 \lambda_q + \lambda_s^{-2} \lambda_q^{-1}) \gamma_s^2 C_{\mathrm{B}}^s F_\Xi + (\lambda_s^3 + \lambda_s^{-3}) \gamma_s^3 C_{\mathrm{B}}^s F_\Omega \Big\} \,, \tag{75}$$

where the kaon, hyperon, cascade and omega degrees of freedom are included. Here T is the freeze-out temperature. The phase space factors F_i of the strange particles are (with g_i describing the statistical degeneracy):

$$F_i \;\; = \;\; \sum_j g_{i_j} W(m_{i_j}/T) \,. \tag{76}$$

In the resonance sums $\sum_j$ all known strange hadrons should be counted. The function $W(x)$ arises from the phase-space integral of the different particle distributions $f(\vec{p})$. For the Boltzmann particle phase space (appropriate when the final state mass is equal or greater than the temperature of the source) and when the integral includes the entire momentum range, we have

$$W(x) \equiv (4\pi)^{-1} \int d^3(p/T) f(\vec{p}) = x^2 \mathrm{K}_2(x) \,, \tag{77}$$

where as before $x = m/T$ and $\mathrm{K}_2(x)$ is the modified Bessel function.

There is a strong constraint between the two fugacities λ_q and λ_s arising from the requirement of strangeness conservation among the final state particles, which was discussed at length recently.[4,5] The non-trivial relations between the parameters characterizing the final state are in general difficult to satisfy and the resulting particle distributions are constrained in a way which differs considerably between different reaction scenarios which we have considered in detail: the rapidly disintegrating QGP or the equilibrated HG phase. These two alternatives differ in particular by the value of the strange quark chemical potential μ_s:

1. In a strangeness-neutral QGP fireball μ_s is always exactly zero, independent of the prevailing temperature and baryon density, since both s and $\bar{s}$ quarks have the same phase-space size.

2. In any state consisting of locally confined hadronic

   clusters, μ_s is generally different from zero at finite baryon density, in order to correct the asymmetry introduced in the phase-space size by a finite baryon content.

At non-zero baryon density, that is for $\mu_B \equiv 3\mu_q \neq 0$, there is just one (or perhaps at most a few) special value $\mu_B^0(T)$ for which $\langle s \rangle = \langle \bar{s} \rangle$ at $\mu_s = 0$, which condition mimics the QGP. We have studied these values carefully[5] for the final state described by Eq. (75): the condition of strangeness conservation takes the simple analytical form[4,5,7]

$$\mu_q^0 = T\cosh^{-1}\left(R_C^s \frac{F_K}{2F_Y} - \gamma_s \frac{F_\Xi}{F_Y}\right), \quad \text{for } \mu_s = 0 \ . \tag{78}$$

Here, and when we consider relative abundance of particles, only the ratio

$$R_C^s = C_M^s / C_B^s \tag{79}$$

appears. We note that there is at most one non-trivial real solution of Eq. (78) for monotonous arguments of $\cosh^{-1}$, and only when this argument is greater than unity.

Clearly, the observation[4,53] of $\lambda_s = 1$ ($\mu_s = 0$) is, in view of the accidental nature of this value in the confined phase, a rather strong indication for the direct formation of final state hadrons from a deconfined phase. In such a process the particle abundances retain memory of the chemical (fugacity) parameters, the conservation of strangeness and other properties is assured by the (non-equilibrium hadronic gas) abundance numbers of the particles produced. For example the number of baryons emitted even at very low temperatures must remain conserved and thus cannot be tiny despite the thermal suppression factor $e^{-m/T}$ — a big change in chemical potentials would require lengthy reequilibration. These effects are absent since $\lambda_s = 1$, at least in the strangeness chemical potential: for the S–W/Pb collisions at 200A GeV this was found already in the first data analysis[14] and this remarkable result was corroborated by an extensive study of the resonance decays and flow effects.[4,5] For the S–S collisions

at 200A GeV a further refinement[53] which allows for a rapidity dependence of λ_q due to flow further underpins the finding $\lambda_s = 1$.

We can thus safely conclude that strange particles produced in 200A GeV Sulphur interactions with diverse targets indicate a particle source which displays a symmetry in phase space size of strange and antistrange particles, which fact is more than just an accident of parameters considering that it appears for two widely different collision systems, S–S and S–W/Pb. A natural explanation is that such a source is deconfined, and that it disintegrates so rapidly, that its properties remain preserved in emitted strange particles. It will be very interesting to see, if this behavior will be confirmed in the Pb–Pb system, with present experiments operating at 158A GeV and possibly later at different collision energies.

We now explore the values of the parameter R_C^s. We consider the constraint imposed by Eq. (78), taking $\gamma_s = 0.7$ (the deviation from unity is of little numerical importance), $\lambda_s = 1$. For λ_q we take three values in Fig. 29: the solid line is for $\lambda_q = 1.5$, choice motivated by the case of S–W/Pb collisions at 200A GeV, the long-dashed line is for $\lambda_q = 1.6$ suitable for the case of Pb–Pb 160A GeV collisions; the short-dashed curve is for $\lambda_q = 2.5$, the value which our model calculations suggest for the 40A GeV collisions (see table 1). The value $R_C^s = 1$ is found for $T \leq 200$ MeV at $\lambda_q \simeq 1.48$–1.6. For lower disintegration temperatures we would have $R_C^s < 1$, as shown in Fig. 29.

The physical observable which we find to be primarily sensitive to the parameter R_C^s, and to a lesser degree to the other thermal model parameters, is the kaon to hyperon abundance ratio at fixed $m_\perp$:

$$R_K|_{m_\perp} \equiv \frac{K_S^0}{\Lambda + \Sigma^0} \,. \tag{80}$$

When computing this ratio, we have incorporated the decay pattern of all listed resonances numerically and included the descendants of strong and weak decays in order to facilitate comparison below with experimental data. In Fig. 30 we show $R_K|_{m_\perp}$ as function of R_C^s for $\lambda_q = 1.5, 1.6, 2.5$, with the same line conventions as in the Fig. 29. We assumed that the distribution of parent particles for kaons and hyperons is according to the thermal equilibrium condition evaluated at temperature implied by Fig. 29.

There is no officially reported value for the R_K ratio. However, WA85 collaboration[30] has presented results for the yields of Λ, $\overline{\Lambda}$ and K_S obtained in S–W collisions at 200A GeV, shown here in Fig. 7, in the interval $1.1 < m_\perp < 2.6$ GeV for the central rapidity region $2.5 < y < 3$. No cascading corrections were applied to these experimental results. From these results we obtain $R_K|_{m_\perp} = 0.11 \pm 0.02$. This implies a far off-HG-equilibrium result $R_C^s = 0.38$ as can be seen in Fig. 30, which according to Fig. 29 leads to a freeze-out temperature $T_f \simeq 145$ MeV. The equilibrium HG source with $R_C^s \simeq 1$ ($R_K|_{m_\perp} \simeq 0.3$) is experimentally completely excluded. The factor $R_C^s \neq 1$ confirms the expectation that these strange particles are produced in non-equilibrium processes — in our model they originate from directly disintegrating
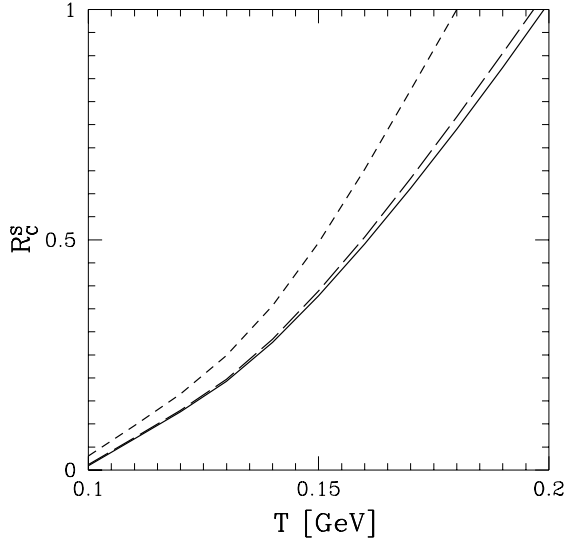
Figure 29: Strangeness neutrality line: R_C^s versus freeze-out temperature for $\lambda_q = 1.5$ (solid line), $\lambda_q = 1.6$ (long-dashed line) and $\lambda_q = 2.5$ (short-dashed line).
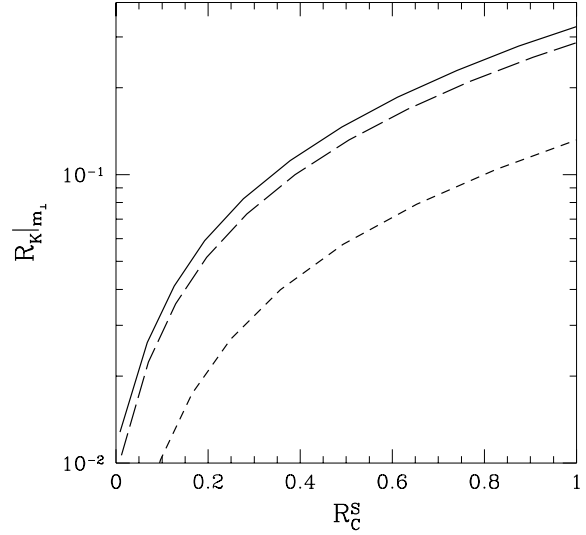
Figure 30: $R_K|_{m_\perp}$ as function of R_C^s for $\lambda_q = 1.5$ (solid line), $\lambda_q = 1.6$ (long-dashed line) and $\lambda_q = 2.5$ (short-dashed line).

QGP fireball. Strangeness conservation constraint fixes the freeze-out condition at $T \simeq 145$ MeV.

The final issue is how, from the value $R_C^s \simeq 0.4$, we can infer the values of the abundance constants $C_M^{'s}$ and $C_B^{'s}$ which (see Eqs. (75, 79)) express the relative strange meson and baryon production abundance to the thermal equilibrium values. If we argue that the strange meson abundance, akin to total meson abundance is enhanced by factor two (i.e. $C_M^{'s} = 2$) as we found studying the entropy enhancement,[7] then the conclusion would be that the strange baryons are enhanced (against their tiny HG equilibrium abundance at $T_f \simeq 145$ MeV) by the factor $C_B^{'s} = 5$.

8   Final State Strange Particle Yields

The ratios of strange baryon to strange antibaryon abundance, looking at the same type of particles, depends only on the chemical properties of the source. We show in Fig. 31 the three ratios and also $\bar{p}/p$. Since we assume $\lambda_s = 1$, we obtain here in particular $R_\Omega = \lambda_s^{-6} = 1$. However, since some re-equilibration is to be expected towards the HG behavior $\lambda_s > 1$, we expect $\lambda_s = 1 + \epsilon$, with ϵ small, and thus for this ratio $R_\Omega = 1 - 6\epsilon < 1$. A further non negligible correction is due to the isospin asymmetry.[4]

We next present the particle ratio results assuming $\gamma_s = 1$ appropriate for a relatively large, long-lived system created in central collisions of largest available nuclei. In the Figs. 32–34 we show three ratios and for each ratio three results: solid lines depicts the result for the full phase space coverage, short dashed line for particles
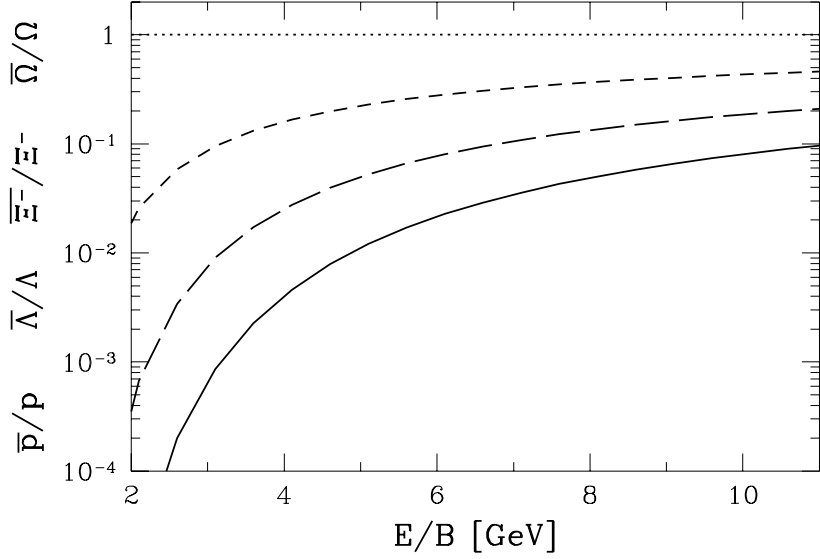
Figure 31: Antibaryon to baryon abundance ratios as function of energy per baryon E/B in a QGP-fireball: $R_N = \bar{p}/p$ (solid line), $R_\Lambda = \overline{\Lambda}/\Lambda$ (long-dashed line), $R_\Xi = \overline{\overline{\Xi}}/\Xi$ (short-dashed line) and $R_\Omega = \overline{\Omega}/\Omega$ (dotted line)
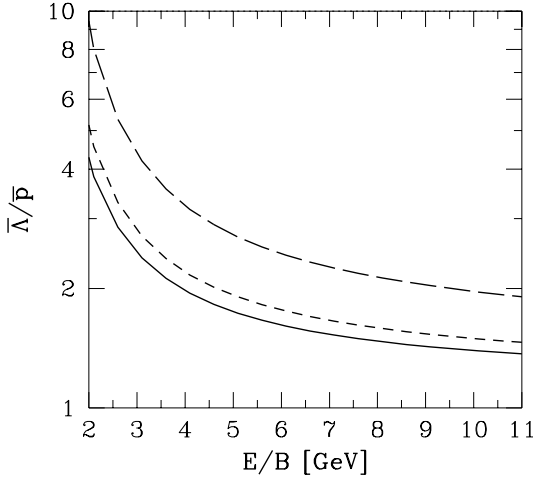
Figure 32: Strange antibaryon ratio $\overline{\Lambda}/\overline{p}$, as function of E/B in a QGP-fireball for $\gamma_s = 1$; solid lines are for full phase space coverage, short dashed line for particles with $p_\perp \geq 1$ GeV and long dashed line for particles with $m_\perp \geq 1.7$ GeV.
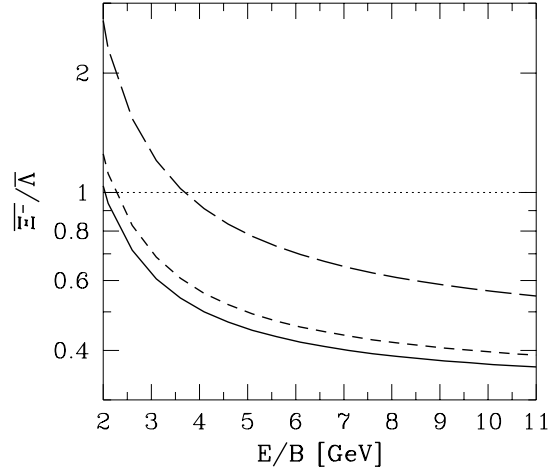
Figure 33: Strange antibaryon ratio $\overline{\overline{\Xi^-}}/\overline{\Lambda}$ for $\gamma_s = 1$, with the same conventions as in Fig. 32.

with $p_\perp \geq 1$ GeV and long dashed line for particles with $m_\perp \geq 1.7$ GeV. In Fig. 32 we show the ratio $\overline{\Lambda}/\overline{p}$, in Fig. 33 the ratio $\overline{\overline{\Xi^-}}/\overline{\Lambda}$ and in Fig. 34 the ratio $\overline{\Omega}/\overline{\Xi^-}$. Because λ_q rises with decreasing E/B and we have kept $\gamma_s = 1$, we find that these three ratios increase as the collision energy is reduced.

The behavior of particle ratios shown in Figs. 32–34 may be of considerable importance, since in reaction models in which QGP is not assumed and the particles are

49
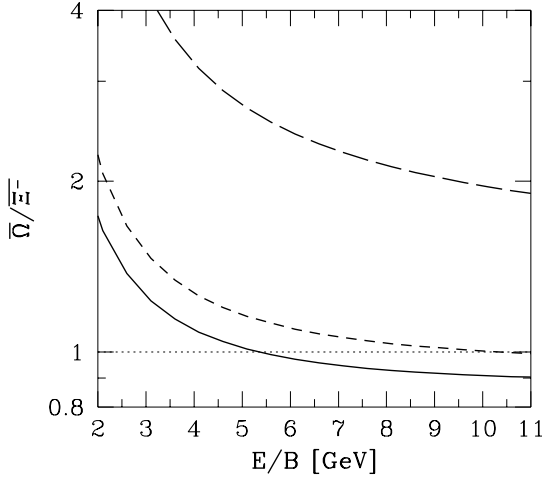
Figure 34: Strange antibaryon ratio $\overline{\Omega}/\overline{\Xi^-}$ for $\gamma_s = 1$, with the same conventions as in Fig. 32.
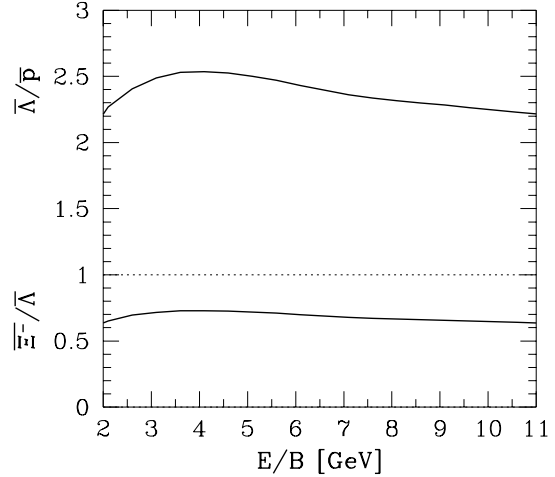
Figure 35: Fixed $m_\perp$ $\overline{\Lambda}/\overline{p}$ and $\overline{\Xi^-}/\overline{\Lambda}$ as function of E/B in the Pb–Pb fireball, taking into account variation of γ_s shown in Fig. 26.

made in a sequence of microscopic collisions these ratios *do increase* from production thresholds with the collision energy, reflecting in this behavior the phase space factors inherent in the reaction cross section. There can be little doubt that this behavior will be observed in relatively low energy heavy ion collisions. At some *transition* energy a jump in particle abundance ratio to the here presented yields should be seen. It is worthwhile to note that even when we incorporate in these strange antibaryon ratios in Fig. 35 the variation of γ_s shown in Fig. 26, we still retain the remarkable behavior that the ratios do not decrease with decreasing energy down to the energy thresholds for the production of the (multi)strange(anti)baryons. Fig. 35 shows actually the worst case scenario, since as we have discussed, the current strangeness production processes and/or fireball expansion lead to an underestimate of the strange phase space saturation.

As a final step in this discussion we present now the analysis of the available and very recent WA85 Ω/Ξ^- production ratio[54] and the $\overline{\Lambda}/\bar{p}$ ratio of the NA35 collaboration obtained for the S–Au system at 200A GeV.[29] Fig. 36 shows a comparison of our ab initio calculation and the pertinent experimental results. We use the same cuts on the range of $p_\perp$ as in the experiment: the experimental points show the results $\overline{\Lambda}/\bar{p} \simeq 0.8 \pm 0.25$ (NA35) for full phase space, $\overline{\Xi^-}/\overline{\Lambda} = 0.21 \pm 0.02$ (WA85) for $p_\perp > 1.2$ GeV; and $(\Omega + \overline{\Omega})/(\Xi^- + \overline{\Xi^-}) = 0.8 \pm 0.4$ (WA85) for $p_\perp > 1.6$ GeV. The chosen values $\gamma_s = 0.70$ and $\eta_p = 0.5$ also bring about good agreement of our model with the precise value of $\overline{\Xi^-}/\overline{\Lambda}$. Fig. 36 shows also the impact of the change of the collision energy on these results, using 50% stopping, rather than $\eta = 1$ used in Figs. 32–34.

Considering that we have computed here everything in an ab initio dynamical model (which as discussed above has some tacit and explicit parameters such as the QCD coupling $\alpha_s = 0.6$ etc., chosen to be in agreement with the earlier experimental results) it is remarkable that such a good agreement with the two very recent results could be attained. We can conclude that the fact that the two ratio $\overline{\Lambda}/\bar{p}$ (NA35)
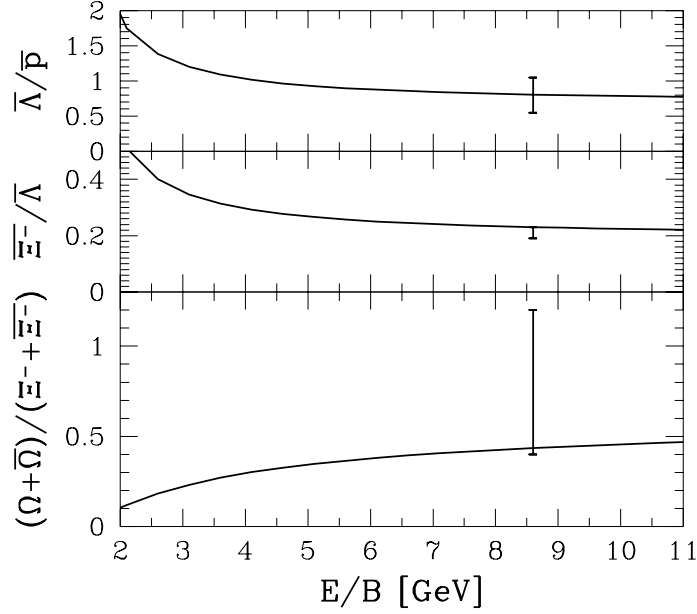
Figure 36: Strange antibaryon ratios for S–W/Pb collisions as function of E/B in a QGP-fireball: $\overline{\Lambda}/\overline{p}$ (full phase space), $\overline{\Xi^-}/\overline{\Lambda}$ for $p_\perp > 1.2$ GeV and $(\overline{\Omega} + \Omega)/(\overline{\Xi^-} + \Xi^-)$ for $p_\perp > 1.6$ GeV; experimental results shown are from experiments NA35, WA85.

and $(\Omega + \overline{\Omega})/(\Xi^- + \overline{\Xi^-})$ (WA85) are satisfactorily explained, provides a very nice confirmation of the consistency of the thermal QGP fireball model.

An interesting question which arises quite often is how the individual particle and in particular total antibaryon yields vary with energy. Eq. (75) allows to determine the absolute particle yields as function of fireball energy. Considerable uncertainty is arising from the off-equilibrium nature of the hadronisation process, which in particular makes it hard to estimate how the different heavy particle resonances are populated, and also, how the abundance factors C_B^s vary as function of energy. Some of this uncertainties are eliminated when we normalize the yields at an energy, which we take here to be the value $E/B = 2.6$ GeV which is applicable to the AGS experiments. In Fig. 37 the so normalized yields of antibaryons taking the freeze-out temperature $T = 150$ MeV are shown (we also assume $\gamma_s = 1$, $\eta_p = 1$ and absence of any re-equilibration after particle emission/production). These yields are rising in qualitatively similar systematic fashion with energy, as would be expected from the microscopic considerations, but the rise of more strange antibaryons is less pronounced. The quantitative point to note is that at AGS ($E/B = 2.6$ GeV) the yield from a disintegrating QGP-fireball is a factor 100–400 smaller compared to yields at $E/B = 9$ GeV. Since the particle rapidity density dN/dy is not that much smaller at the lower energies (recall that the specific entropy, see table 1, drops only by factor 3.5, implying a reduction in specific multiplicity by a factor 5), it is considerably more difficult at the lower energies to search for antibaryons than it is at higher energies. We should remember that the results presented in Fig. 37 are obtained assuming for-
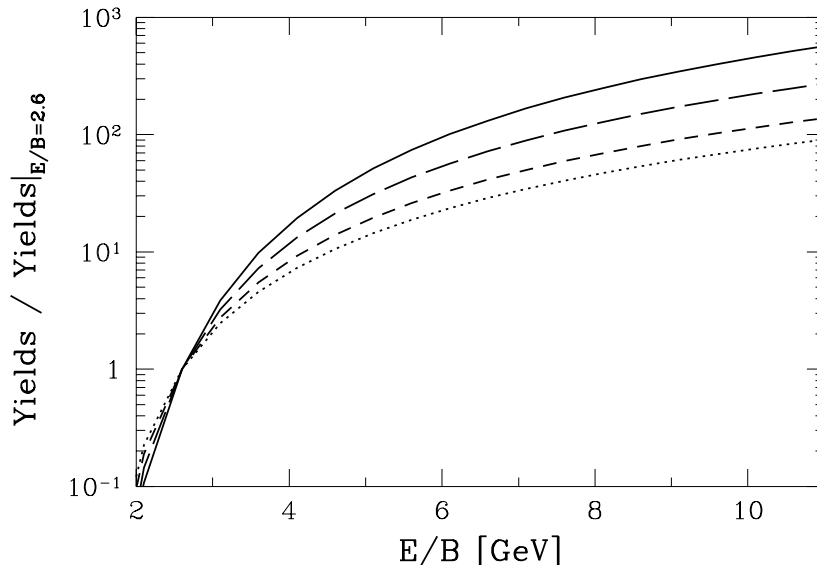
Figure 37: Relative antibaryon yields as function of E/B in a QGP-fireball. $\overline{p}$ (solid line), $\overline{\Lambda}$ (long-dashed line) $\overline{\Xi^-}$ (short-dashed line) and $\overline{\Omega}$ (dotted line), all normalized to their respective yields at $E/B = 2.6$ GeV .

mation of the QGP-fireball and same freeze-out and hadronisation conditions for all energies shown.

9   Summary and Conclusions

We have described in detail how production and final state manifestation of the heavy flavors, in particular strangeness, can help today to identify and study the properties of the deconfined phase. Our exploration of thermal charm production has shown that open charm could become an interesting probe of initial conditions reached at LHC energies.

Our primary objective in this work was to establish the systematic behavior of the heavy flavor production, the associated antibaryon yields and to determine the freeze-out conditions of these particles given that the experimental results suggest that the thermal (kinetic) equilibrium is established, while the chemical (particle abundance) equilibrium in the processes governing final state particle freeze-out is maybe just not achieved. Motivated by the absence of chemical particle abundance equilibrium, we employed here a picture of final state hadron production which involves rapid disintegration of the QGP-fireball. Central to the particle abundances are then the chemical properties of the QGP-fireball and we have discussed these comprehensively as function of collision energy and stopping.

We have presented a simple model, which allows to determine, in a systematic fashion, the thermal conditions reached in high density deconfined matter generated in heavy ion collisions. It is based on the observation that during the collision the

52

compression of the quark-gluon matter can proceed until the internal pressure exerts sufficiently strong counter balancing force. We have shown that the thermal conditions we find at the end of strangeness chemical equilibration in the fireball (see bottom of table 1) are in good agreement with our expectations derived from particle yields seen in S–Pb/W collisions. To wit we needed to make a reasonable choice of the physical parameters: at $T = 250$–300 MeV we took $\alpha_s = 0.6$; for stopping we adopted $\eta = 50\%$, about equal for baryon number, energy and momentum. Given these assumptions, we were able to study the current strange particle data at 200A GeV and have reached good agreement with experiment.

We studied in detail the production and evolution of strangeness in a dynamical QGP fireball evolution model. As expected we found that the large strangeness abundance produced in the early stages needs not to be reannihilated rapidly. Contrary to earlier studies we have determined that strangeness can overpopulate the available phase space at plasma disintegration, and thus strange antibaryon abundances could show $\gamma_s > 1$. Of course, if plasma expansion were to go very slowly, this freeze-out phenomenon would not occur, and strangeness would be reannihilated. However for low temperature cross over to hadronic matter the evolution of the fireball can overwhelm the strangeness annihilation process leading to oversaturated phase space with $\gamma_s > 1$. Our calculations have thus shown that that γ_s is not only a probe of the initial temperature and size of the fireball, but is also a sensitive probe of the final freeze-out conditions.

Our results imply that many features of strange particle production results obtained at 200A GeV, are consistent with the QGP hypothesis of the central, thermal fireball. However, we believe that in order to ascertain the possibility that indeed the QGP phase is already formed at 200A GeV a more systematic exploration as function of collision energy of these observables would be needed — conclusions drawn from a small set of experimental results suffer from the possibility that some coincidental and unknown features in the reaction mechanisms could simulate just the observed QGP-like properties. It is highly unlikely that this would remain the case, should a key feature such as collision energy be varied.

We have therefore computed in a systematic fashion the behavior of strange particle yields assuming conditions likely to occur in Pb–Pb interactions as function of energy and/or impact parameter. It is most interesting that these results show patterns of behavior which could indeed be unique for the QGP type of fireballs — in particular, the relative yields of strange antibaryons rise with decreasing energy. We are persuaded that such pattern of behavior could not occur for a wide range of energy for normal confined matter, where the rise in cross sections with energy dominates particle yields.

We stress that our description and hence the anomalous behavior of particle production discussed here is based on collective mechanisms (QGP-fireball), which is intrinsically different from microscopic approaches, in particular when these are based on a hadronic cascade picture. Such models generally exploit specific data and/or extrapolations and assumptions about individual hadronic reactions and their cross sections. We note that no alternative model to the here developed rapidly hadronising

QGP has been proposed which could generate all features known today for S–W/Pb collisions. For example we note the dual parton model,[47] which finds a small value for the relative abundance $\overline{\Omega}/\overline{\Xi}$, and generally produces dips in the central rapidity region for the strange antibaryon yields.

Given the results we have obtained here, we conclude that experimental data on strange (anti)baryon production provides the best hadronic signatures, and diagnostic tools, of the deconfined matter. We stress again the large ratios in the QGP-fireball reaction picture, such as $\overline{\Lambda}/\bar{p}$, $\overline{\Xi}/\overline{\Lambda}$ which we have found at relatively small energies — in microscopic models and near to $\overline{\Lambda}$, $\overline{\Xi}$ production thresholds in p–p interaction this ratios should be very small. This lets us expect that there will be a sudden rise in the relative $\overline{\Lambda}/\bar{p}$, $\overline{\Xi}/\overline{\Lambda}$ yields as function of collision energy which will provide an interesting possibility to identify the energy at which collective production of (strange) antibaryons is first encountered. At this energy we should also encounter for the first time the other features of the QGP phase: strangeness production enhancement, strange phase space saturation $(\gamma_\mathrm{s} \to 1)$, and possibly oversaturation $\gamma_\mathrm{s} > 1$, entropy enhancement (particle multiplicity enhancement), pattern of strange antibaryon flow showing $\lambda_\mathrm{s} = 1$. It seems that the discovery of the deconfined QGP-phase of hadronic matter is just around the corner.

10   Discussion

Q — Herbert Ströbele: $\overline{\Xi}/\overline{\Lambda}$ decreases with E/B in your model. Is such a behavior possible or probable in hadronic models?

A: In our model we have $\overline{\Xi}/\overline{\Lambda} \propto \gamma_\mathrm{s}\lambda_\mathrm{q}$, which is generally true in every statistical model, since this ratio is sensitive both to the baryon density and the degree of chemical strangeness equilibration. However, calculations show that the formation in confined hadronic matter of heavy and complex strange antibaryons is rather difficult, with abundances being far off the statistical equilibrium. Thus we expect this special ratio to be rising slowly from zero, at particle production threshold energies, yielding the intuitive result that the abundance ratio $\overline{\Xi}/\overline{\Lambda}$ increases continuously with CM energy. Particle cascade model calculations have led to this qualitative expectations and thus we are led to believe that the behavior we found for QGP is qualitatively different from confined hadronic model predictions.

Q — Carlos Bertulani: How do you incorporate in-medium corrections in the strangeness production cross section? Don't they change their energy dependence?

A: Since our calculations here address the QGP phase we have the possibility that the QCD coupling constant is medium dependent, $\alpha_\mathrm{s}(q^2) \to \alpha_\mathrm{s}(T, \lambda_\mathrm{q})$. In the perturbative approach we are using the value of α_s at the typical computed values of q^2 with given environmental conditions. The medium effect is implicitly accounted for at the level of the first order perturbation theory. However, to reach greater precision we would have to properly account for medium effects, in particular by computing the reaction matrix elements resuming the radiative correction diagrams, evaluated in the medium.

Q — Horst Stöcker: The critical issue in the model is the (arte)fact that the transition from QGP to Hadrons does *not* allow for (sea) quark production in hadronisation (u, d, s produced in flux-tube) and neglects entirely meson ($q\bar{q}$) production from gluon decay.

If these effects would be considered, all ratios, fugacities etc. would come out completely differently.

A: We totally disagree with the conclusion you present without a calculational setting for the here considered particles such as $\overline{\Xi}$, $\overline{\Lambda}$, Ξ etc. . The study of these particle ratios produced in the sudden recombination-fragmentation model, including in particular also gluon fragmentation, was published by J. Rafelski and M. Danos,[15] where it was shown that the fragmentation of gluons is not impacting the strange antibaryon ratios observed at high $m_\perp > 1.5$ GeV here considered. This happens for two reasons: first, the overall abundance is only little (20%) changed, since the fragmentation of gluons populates light and strange flavors with similar weight as is found in the QGP for the recombination. Second, this effect is even less pronounced in the data we consider in this report, since 'hard' final hadrons are made more easily in recombination, given that fragmentation shifts the produced particles to lower $m_\perp$ (the available energy is split into two parts). It is possible that this is the reason why the fragmenting string models studied by your Frankfurt group yield too soft transverse distributions of these particles.

On the other hand we agree with the implication of your remark that the gluon and other fragmentation is an important process populating soft hadrons of low mass, in particular pions. Through these mechanism the entropy is conserved or increased at the cross over point of the phases.[7] We are well aware of these phenomena, not relevant in our here presented work on strange antibaryons.

Q — Larry McLerran: Shouldn't γ be energy dependent?

A: Strictly speaking, given the way we introduced into our description the parameter γ it cannot be a function of the momentum and thus energy of the emitted particles — this we have opted for considering that thermal equilibrium is more rapidly established than is the chemical equilibrium. Thus in our approach γ is a statistical parameter that is established in the fireball, given the collision conditions. It can depend on the history of the fireball and hence, e.g., on initial temperature and thus on the collision energy of the ions.

Acknowledgment

References

1. C. DeTar, *Quark Gluon Plasma in Numerical Simulations of lattice QCD*, U. Utah Preprint, to appear in *Quark Gluon Plasma 2*, R.C. Hwa (Eds.), World Scientific,

Singapore.

T. Blum, L. Kärkkäinen, D. Toussaint, S. Gottlieb, *Phys. Rev.* D **51**, 5153 (1995).

2. *Strangeness in Hadronic Matter: S'95* Proceedings of Tucson workshop, January 1995, American Institute of Physics Proceedings Series Vol. **340**, New York, 1995, edited by J. Rafelski.

3. J. Rafelski, *Phys. Rep.* **88**, 331 (1982).

4. J. Letessier, A. Tounsi, U. Heinz, J. Sollfrank and J. Rafelski, *Phys. Rev.* D **51**, 3408 (1995); J. Sollfrank, M. Gaździcki, U. Heinz and J. Rafelski, *Z. Physik* C **61**, 659 (1994).

5. J. Letessier, J. Rafelski and A. Tounsi, *Phys. Lett.* **B321**, 394 (1994).

6. J. Rafelski and R. Hagedorn, in: *Statistical Mechanics of Quarks and Hadrons*, edited by H. Satz, North Holland, Amsterdam 1981, pp. 253–272;
J. Rafelski, in: *Workshop on Future Relativistic Heavy Ion Experiments*, edited by R. Bock and R. Stock, GSI-Yellow Report 81-6, Darmstadt 1981, pp. 282–324;
J. Rafelski, *Phys. Rep.* **88**, 331 (1982);
M. Jacob and J. Rafelski, *Phys. Lett.* B **190**, 173 (1987).

7. J. Rafelski, J. Letessier and A. Tounsi, *XXVI International Conference on High Energy Physics*, Dallas, Texas, 1992, AIP-Conference Proceedings No 272, p. 983, edited by J.R. Sanford; J. Letessier, A. Tounsi, U. Heinz, J. Sollfrank and J. Rafelski, *Phys. Rev. Lett.* **70**, 3530 (1993); M. Gaździcki, *Z. Physik* C **66**, 659 (1995).

8. *Hot Hadronic Matter*, Proceedings of NATO-Advanced Research Workshop held in Divonne, France, June 1994, edited by J. Letessier, H.H. Gutbrod and J. Rafelski, NATO Physics series Vol. B **346**, Plenum Press, New York 1995.

9. I. Otterlund, *Physics of Relativistic Nuclear Collisions*, in[10] p. 57.
S.P. Sorensen *et al.*, *Nuclear Stopping Power*, in: *Proc. XXI Int. Symposium on Multiparticle Dynamics 1991*, World Scientific, Singapore, 1992.

10. *Particle Production in Highly Excited Matter*, Proceedings of IlCiocco NATO Summer School, July 1992, edited by H.H. Gutbrod and J. Rafelski, NATO Physics series Vol. B **303**, Plenum Press, New York, 1993.

11. A. Schnabel and J. Rafelski, *Phys. Lett.* B **207**, 6 (1988); and
in *Proceedings of the 3rd Conference on the Intersection between Particle and Nuclear Physics*, Rockport, 1988, G. Bunce, ed., AIP Proceedings Series No. 176, p. 1068, New York, l988.

12. H.-C. Eggers and J. Rafelski, *Int. J. Mod. Phys.* **A6**, 1067 (1991) (see in particular Fig. 8).

13. J. Letessier, J. Rafelski and A. Tounsi, *Phys. Lett.* B **333**, 484 (1994).

14. J. Rafelski, *Phys. Lett.* B **262**, 333 (1991); *Nucl. Phys.* A **544**, 279c (1992).

15. J. Rafelski and M. Danos, *Phys. Lett.* **B192**, 432 (1987); *Phys. Rev.* **D27**, 671 (1983).

16. T. S. Biró and J. Zimányi, *Nucl. Phys.* **A395**, 525 (1983).

17. L. P. Csernai and I. N. Mishustin, *Phys. Rev. Lett.* **74**, 5005 (1995).

18. J. Rafelski and M. Danos *Phys. Rev.* C **50**, 1684 (1994);
    J. Letessier, J. Rafelski and A. Tounsi, *Phys. Lett.* B **328**, 499 (1994);
    J. Stachel *et al.*, in[8] and private communication.

19. K. S. Lee, U. Heinz, and E. Schnedermann, *Z. Physik* **C48**, 525 (1990);
    E. Schnedermann and U. Heinz, *Phys. Rev. Lett.* **69**, 2908 (1992); and *Phys. Rev.* **C47**, 1738 (1993);
    E. Schnedermann, J. Sollfrank, and U. Heinz, in[10] p. 175.

20. M. Kataja, J. Letessier, P.V. Ruuskanen and A. Tounsi, *Z. Physik* C **55**, 153 (1992).

21. E. Quercigh, in[10] p. 175.

22. M. Gaździcki, private communication.

23. S. Abatzis *et al.* (WA94 collab.), *Phys. Lett.* B **354**, 178 (1995);
    D. DiBari *et al.* (WA85 collaboration), *Nucl. Phys.* A **590**, 307c (1995);
    D. Evans *et al.* (WA85 collab.), *Nucl. Phys.* A **566**, 225c (1994);
    WA85/WA94 collaboration presentations in[2] pp. 223–272;
    F. Antinori, private communication.

24. J. Rafelski, *Phys. Lett.* **B262**, 333 (1991);
    J. Rafelski, *Nucl. Phys.* **A544**, 279c (1992), and references therein.

25. J. Letessier, J. Rafelski and A. Tounsi, *Quark-gluon plasma formation and strange antibaryons.* Preprint AZPH-TH/95-14R and PAR/LPTHE/95-36R, submitted to *Phys. Lett.* B.

26. J. Letessier, J. Rafelski and A. Tounsi, *Energy dependence of strange particle yields from a quark-gluon plasma fireball.* Preprint AZPH-TH/95-13 and PAR/LPTHE/95-24, submitted to *Phys. Rev.* D.

27. N.S. Amelin, L.V. Bravina, L. P. Csernai, V.D. Toneev, K.K. Gudima, S.Yu. Sivoklokov, *Phys. Rev.* C **47**, 2299 (1993);
    H. Sorge, *Phys. Lett.* B **344**, 35 (1995);
    K. Werner, in this volume.

28. T. Åkesson *et al.*, AFS-ISR Collaboration, *Nucl. Phys.* **B246**, 1 (1984).

29. T. Alber et al. (NA35 collab.), preprint IKF-HENPG/5-95, submitted to *Phys. Lett.* B;
    J. Günther *et al.* (NA35 collab.), *Nucl. Phys.* A **590**, 487c (1995).

30. D. Evans for the WA85 collaboration, in[2] p. 234, see Fig. 3; and private communication.

31. P. Bordalo for the NA38 collaboration, in[2] p. 152;
    and *Phys. Lett.* B (in press).

32. R. Santo *et al.* (WA80 collaboration), *Nucl. Phys.* A **566**, 61c (1994);
    R. Albrecht *et al.* (WA80 collaboration), *Production of η Mesons in 200A GeV S+S and S+Au.* Münster Preprint IKP-MS-95/0701;
    K.H. Kampert and H. Gutbrod, private communication.

33. for strange particles see: T. Alber *et al.*, *Z. Physik* C **64**, 195 (1994);
    for protons and pions see J. Beachler *et al.*, *Phys. Rev. Lett.* **72**, 1419 (1994);
    for antiprotons see[29] .

34. S.R. de Groot, W.A. van Leeuwen, Ch.G. van Weert, *Relativistic Kinetic Theory,* North Holland, Amsterdam, 1980.

35. J. Rafelski and B. Müller, *Phys. Rev. Lett.* **48**, 1066 (1982); **56**, 2334E (1986); T. Biró and J. Zimányi, *Phys. Lett* B **113**, 6 (1982); *Nucl. Phys.* A **395**, 525 (1983).

36. T.S. Biró, P. Lévai and B. Müller, *Phys. Rev.* D **42**, 3078 (1990).

37. T. Altherr and D. Seibert, *Phys. Lett.* B **313**, 149 (1993) and Phys. Rev. C **49**, 1684 (1994).

38. N. Bilić, J. Cleymans, I. Dadić and D. Hislop, *Phys. Rev.* C **52**, 401 (1995).

39. J. Sollfrank and U. Heinz *The Role of Strangeness in Ultrarelativistic Nuclear Collisions*, Helsinki preprint HU-TFT-95-27, to appear in *Quark Gluon Plasma 2*, R.C. Hwa (Eds.), World Scientific, Singapore.

40. P. Koch, B. Müller and J. Rafelski, *Z. Physik* A **324**, 453 (1986).

41. J. Letessier, J. Rafelski and A. Tounsi, *Phys. Lett.* B **323**, 393 (1994).

42. J. Letessier, J. Rafelski and A. Tounsi, *Phys. Rev.* C **50**, 406 (1994); J. Rafelski, J. Letessier and A. Tounsi, *Acta. Phys. Pol.* A **85**, 699 (1993).

43. B. Combridge, *Nucl. Phys.* B **151**, 429 (1979); T. Matsui, B. Svetitsky and L.D. McLerran, *Phys. Rev.* D **34**, 783 (1986).

44. I. Gradshteyn and I. Ryzhik, *Table of integrals, series, and products.* Academic Press INC., 1980.

45. P. Levai, B. Müller and X.-N. Wang, *Phys. Rev.* C **51**, 3326 (1995).

46. I. Sarcevic and P. Valerio, *Phys. Rev.* C **51**, 1433 (1995).

47. A. Capella, *Strangeness Enhancement in Heavy Ion Collisions.* Preprint LPTHE Orsay 94-113; A. Capella, A. Kaidalov, A. Kouider Akil, C. Merino, J. Tran Thanh Van, *Strange Baryon Production in Heavy Ion Collisions.* Preprint LPTHE Orsay 95-41, June 1995.

48. P. Koch and J. Rafelski, *Nucl. Phys.* A **444**, 678 (1985).

49. P. Koch, B. Müller, and J. Rafelski, *Phys. Rep.* **142**, 167 (1986).

50. T. Alber *et al.* (NA 35 Collaboration), *Z. Physik* C **66**, 77 (1995).

51. H.W. Barz, B.L. Friman, J. Knoll and H. Schulz, *Nucl. Phys.* A **484**, 661 (1988); *Nucl. Phys.* A **519**, 831 (1990).

52. For an overview see J. Zimányi *et al.*, in[10] p. 243.

53. C. Slotta, J. Sollfrank and U. Heinz, in[2].

54. F. Antinori, in[2]; S. Abatzis *et al.* (WA85 collaboration), *Phys. Lett.* B **316**, 615 (1993); *Phys. Lett.* B **347**, 158 (1995).

55. H. Grote, R. Hagedorn and J. Ranft, *Particle Spectra*, CERN black report (1970).